Chapter 3

FEM with Magnetostrictive Actuators and Sensors

3.1 Introduction

In the last chapter, various material models (linear, nonlinear, coupled and uncoupled) were formulated and the range of its applicability were discussed. In this chapter, these will be incorporated in the conventional 3-D Finite Element (FE) formulation. From the 3-D FE models, 1-D and 2-D models will be deduced and the effect of different material models on the healthy and damaged 1-D and 2-D laminated composite structures will be investigated. In particular, the impact of different material models on the SHM studies will be highlighted.

3.1.1 Existing Literature

There is a very few literature available on the FE formulation for composite structure with embedded magnetostrictive patches. Kannan and Dasgupta [174] developed quasi-static Galerkin finite-element theory for modelling magneto-mechanical interactions at the macroscopic level considering body forces and coupled constitutive nonlinearities. Benbouzid et al. modelled the static [35] and dynamic [37] behavior of the nonlinear magneto-elastic medium for magneto-static case using finite element method. Magneto-mechanical coupling was incorporated considering both permeability and elastic modulus as functions of stress and magnetic field. In reference [38], finite elements were used for modelling different magnetic circuits with leakage flux of a basic actuator configuration. However, none has provided a convenient way for analysis of magnetostrictive smart structure considering coupled magneto-mechanical features.

In this chapter, a new finite element formulation for structures with in-built magnetostrictive patches that can handle coupled analysis is presented. Here, both magnetic and mechanical degrees are considered as unknown degrees of freedom. In the present approach, smart patches are introduced in the laminates to induce actuation strains on the application of magnetic field. This changes the state of stress in the sensing patch and hence the magnetic flux density through enclosed magnetic coil changes, resulting in a voltage across the sensing coil.

Next these elements are used for structural health monitoring applications and shown that sensitivity of damage in open circuit voltages for SHM is comparable with the error induced due to uncoupled assumption in the finite element analysis. Finally this chapter concludes that for the SHM application with magnetostrictive sensor and actuator, coupled analysis is required for true estimation of the response of the structure.

This chapter is organized as follows. First the variational formulation is given to obtain the mass, stiffness and coupling stiffness of the system. The main aim of the study is to bring out the effect of magneto-mechanical coupling on the overall response of laminated composite structure. For this purpose numerical study is performed on composite structures containing two patches, one acting as an actuator and the other as a sensor for varying current amplitude and ply sequence. Both static, frequency response and time response analysis are performed to bring out the essential difference in responses between coupled and uncoupled models. The chapter is then concluded with a brief summary.

3.2 3D Finite Element Formulation

Finite element formulation begins by writing the associated energy in terms of nodal degrees of freedom by assuming the displacement and magnetic field variation over each element. That is, the displacement field $\{U\}$ can be written as

$$\{U\} = \{u \quad v \quad w\}^T \tag{3.1}$$

where $u(x, y, z, t), v(x, y, z, t)$ and $w(x, y, z, t)$ are the displacement component in x, y and z direction respectively. These displacements are obtained from element nodal displacements $\{U^e(t)\}$, through the element shape function, $[N_U(x, y, z)]$ as

$$\{U\} = [N_U]\{U^e\} \tag{3.2}$$

The strains $\{\epsilon\}$ in terms of displacements $\{U\}$, are obtained as

$$\{\epsilon\} = \{\epsilon_{xx} \;\; \epsilon_{yy} \;\; \epsilon_{zz} \;\; \gamma_{yz} \;\; \gamma_{xz} \;\; \gamma_{xy} \;\; \}^T = [\mathcal{L}]\{U\} \tag{3.3}$$

Where $[\mathcal{L}]$ is given by

$$[\mathcal{L}] = \begin{bmatrix} \frac{\partial}{\partial x} & 0 & 0 \\ 0 & \frac{\partial}{\partial y} & 0 \\ 0 & 0 & \frac{\partial}{\partial z} \\ 0 & \frac{\partial}{\partial z} & \frac{\partial}{\partial y} \\ \frac{\partial}{\partial z} & 0 & \frac{\partial}{\partial x} \\ \frac{\partial}{\partial y} & \frac{\partial}{\partial x} & 0 \end{bmatrix} \tag{3.4}$$

Using Equation-(3.2) in Equation-(3.3), the strains can be written as

$$\{\epsilon\} = [\bar{B}]\{U^e\} \tag{3.5}$$

where $[\bar{B}]$ is strain-displacement matrix and can be expressed as

$$[\bar{B}] = [\mathcal{L}][N_U]. \tag{3.6}$$

Similarly Magnetic field vector in the three coordinate directions $\{H\}$ can be written as

$$\{H\} = \{H_x \quad H_y \quad H_z\}^T \tag{3.7}$$

These magnetic fields are obtained from element nodal magnetic fields $\{H^e\}$, through the shape function, $[N_H(x, y, z)]$ as

$$\{H\} = [N_H]\{H^e\} \tag{3.8}$$

Strain Energy in magnetostrictive material over a volume v is given by,

$$V_e = \frac{1}{2}\int_v \{\epsilon\}^T\{\sigma\}dv$$

Substituting for $\{\sigma\}$ from Equation-(2.9), $\{\epsilon\}$ from Equation-(3.5) and $\{H\}$ from Equation-(3.8), this can be written as

$$\begin{aligned} V_e &= \frac{1}{2}\int_v \{\epsilon\}^T\{[Q]\{\epsilon\} - [e]^T\{H\}\}dv \\ &= \frac{1}{2}\int_v \{\epsilon\}^T[Q]\{\epsilon\}dv - \frac{1}{2}\int_v \{\epsilon\}^T[e]^T\{H\}dv \\ &= \frac{1}{2}\{U^e\}^T\left[K_{UU}\right]\{U^e\} - \frac{1}{2}\{U^e\}^T\left[K_{UH}\right]\{H^e\} \end{aligned} \tag{3.9}$$

where

$$[K_{UU}] = \int_v [\bar{B}]^T [Q][\bar{B}]dv, \qquad [K_{UH}] = \int_v [\bar{B}]^T [e]^T [N_H]dv. \tag{3.10}$$

Where $[K_{UU}]$ is the stiffness matrix associated with mechanical degrees of freedom and $[K_{UH}]$ is the coupling stiffness matrix that couples the mechanical and magnetic degrees of freedoms. Kinetic Energy in magnetostrictive material is

$$T_e = \frac{1}{2}\int_v \{\dot{U}\}^T [\rho]\{\dot{U}\}dv \tag{3.11}$$

where $\{\dot{U}\}$ is velocity vector, ρ is density of the material. Substituting $\{U\}$ from Equation-(3.2), the kinetic energy can be written as

$$\begin{aligned} T_e &= \frac{1}{2}\int_v \{[N_U]\{\dot{U}^e\}\}^T [\rho][N_U]\{\dot{U}^e\}dv \\ &= \frac{1}{2}\{\dot{U}^e\}^T \int_v [N_U]^T [\rho][N_U]dv\{\dot{U}^e\} = \frac{1}{2}\{\dot{U}^e\}^T [M_{UU}]\{\dot{U}^e\} \end{aligned} \tag{3.12}$$

where the mass matrix for mechanical degrees of freedom can be written as

$$[M_{UU}] = \int_v [N_U]^T [\rho][N_U]dv \tag{3.13}$$

Magnetic Potential Energy in magnetostrictive material is given by

$$V_m = \frac{1}{2}\int_v \{B\}^T \{H\}dv \tag{3.14}$$

Substituting $\{B\}$ from Equation-(2.10), $\{\epsilon\}$ from Equation-(3.5) and $\{H\}$ from Equation-(3.8), magnetic potential energy can be written as,

$$\begin{aligned} V_m &= \frac{1}{2}\int_v \{[e]\{\epsilon\} + [\mu^\epsilon]\{H\}\}^T \{H\}dv \\ &= \frac{1}{2}\{U^e\}^T [K_{UH}]\{H^e\} + \frac{1}{2}\{H^e\}^T [K_{HH}]\{H^e\} \end{aligned} \tag{3.15}$$

where $[K_{HH}]$ is stiffness matrix of magnetic degrees of freedom, which can be expressed as

$$[K_{HH}] = \int_v [N_H]^T [\mu^\epsilon]^T [N_H]dv. \tag{3.16}$$

Magnetic External Workdone for N turn coil with coil current I, is given by

$$W_m = IN\int_A \{[\mu^\sigma]\{H\}\} \; . \; dA \tag{3.17}$$

If n is the coil tern per unit length, A is the cross sectional area of the magnetostrictive patch and $\{l_c\}$ is the direction cosine vector of coil axis, the above expression can be written as

$$\begin{aligned} W_m &= In\{l_c\}^T \int_v [\mu^\sigma]\{H\}dv \\ &= \{F_H\}^T\{H^e\} \end{aligned} \tag{3.18}$$

where $\{F_H\}$ is given by

$$\{F_H\} = In\{l_c\}^T \int_v [\mu^\sigma][N_H]dv \tag{3.19}$$

Mechanical External Workdone is

$$\begin{aligned} W_e &= \int_v \{b\}^T\{U\}dv + \int_S \{\tau\}^T\{U\}dS \\ &= \{R\}^T\{U^e\} \end{aligned} \tag{3.20}$$

where $\{b\}$ is body force vector. and $\{\tau\}$ is surface force vector acting on an area S. $\{R\}^T$ is equivalent nodal load for external mechanical forces of the magnetostrictive material.

Applying the Hamilton's Principle $\partial(\int_{t_1}^{t_2}(T_e - V_e + V_m + W_m + W_e)dt) = 0$, we can the governing FE equation. This takes a varied form for uncoupled and coupled model. These are given below.

3.2.1 Uncoupled Model

In uncoupled model magnetic field, H is considered independent of mechanical condition [216], and is a function of coil current I, which is given by

$$H = k_c I \tag{3.21}$$

Where k_c is coil constant. Hence, in uncoupled model only mechanical degrees of freedom, $\{U^e\}$ are unknowns. Substituting this in the Hamiltonian's Equation, the governing differential equation becomes

$$[M_{UU}]\{\ddot{U^e}\} + [K_{UU}]\{U^e\} = [K_{UH}]\{H^e\} - \{R\} \tag{3.22}$$

Where H_e is calculated using Equation-(3.21).

3.2.2 Coupled Model

Unlike uncoupled model, in the coupled model, the mechanical and magnetic degrees of freedom are considered as unknown. Hence, Hamiltonian's principle gives following Equations.

$$\begin{bmatrix} M_{UU} & 0 \\ 0 & 0 \end{bmatrix} \begin{Bmatrix} \ddot{U}^e \\ \ddot{H}^e \end{Bmatrix} + \begin{bmatrix} K_{UU} & -K_{UH} \\ K_{HU} & K_{HH} \end{bmatrix} \begin{Bmatrix} U^e \\ H^e \end{Bmatrix} = \begin{Bmatrix} -R \\ F_H \end{Bmatrix} \tag{3.23}$$

Note that the generalized stiffness matrix is not a symmetric matrix. Both the equations, sensing and actuation are coupled through the off-diagonal, sub-matrix of the stiffness matrix. Expanding Equation-(3.23), we get

$$[M_{UU}]\{\ddot{U}^e\} + [K_{UU}]\{U^e\} - [K_{UH}]\{H^e\} = -R \tag{3.24}$$

and

$$\begin{aligned} [K_{UH}]^T\{U^e\} + [K_{HH}]\{H^e\} &= \{F_H\}^T \\ or \quad \{H^e\} &= [K_{HH}]^{-1}\{\{F_H\}^T - [K_{UH}]^T\{U^e\}\} \end{aligned} \tag{3.25}$$

Substituting $\{H^e\}$ from Equation-(3.25) in Equation-(3.24) we get

$$[M_{UU}]\{\ddot{U}^e\} + [K_{UU}{}^\star]\{U^e\} = \{F^\star\} \tag{3.26}$$

where

$$\begin{aligned} [K_{UU}{}^\star] &= [[K_{UU}] + [K_{UH}][K_{HH}]^{-1}[K_{UH}]^T] \\ \{F^\star\} &= [K_{UH}][K_{HH}]^{-1}\{F_H\} - \{R\} \end{aligned} \tag{3.27}$$

3.3 Computation of Sensor Open Circuit Voltage

After the computation of nodal displacement and velocities, we can compute the sensor open circuit voltage. This is particularly of great interest in structural health monitoring studies. In this section, we derive the necessary expression for both coupled and uncoupled models.

If the sensor coil current is considered as zero, after determining the mechanical and magnetic degrees of freedom, sensor open circuit voltage can be post processed in both uncoupled and coupled model. Using Faraday's law, open circuit voltage V in the sensing coil can be calculated from magnetic flux passing through the sensing patch.

3.3.1 Uncoupled Model

In the uncoupled model, the nodal magnetic field is zero as per Equation-(3.21) with zero sensor coil current. To get the open circuit voltage, magnetic flux density can be expressed in terms of strain from the sensing equation, (Equation-(2.10)) as

$$\{B\} = [d]\{\sigma\} = [d][Q]\{\epsilon\} = [e]\{\epsilon\} = [e][\bar{B}]\{U^e\} \tag{3.28}$$

Now using Faraday's law, open circuit voltage of the sensor can be calculated as

$$V = -N_s \int_A \frac{\partial}{\partial t}[d]\{\sigma\} \; . \; dA \tag{3.29}$$

This can be converted to volume integration as before and the expression for voltage become

$$V = -n_s\{l_c\}^T \frac{\partial}{\partial t} \int_v [e]\{\epsilon\} dv = \{F_v\}^T \{\dot{U}^e\} \tag{3.30}$$

where $\{F_v\}^T$ for uncoupled model becomes

$$\{F_v\}^T = -n_s\{l_c\}^T \int_v [e][\bar{B}] dv \tag{3.31}$$

3.3.2 Coupled Model

Magnetic flux density is computed from nodal magnetic field, which is obtained from finite element analysis. Thus open circuit voltage in the sensor can be calculated from the expression

$$V = -N_s \int_A -\frac{\partial}{\partial t}\{\mu^\sigma H\} \; . \; dA \tag{3.32}$$

where N_s is the total coil turn of the sensing patch. Dividing by the length of the patch and pre-multiplying with the direction cosine vector of coil axis, the above area integration with dot product is converted to volume integration. Substituting $\{H\}$ from Equation-(3.8), the open circuit voltage can be written as

$$\begin{aligned} V &= n_s\{l_c\}^T \int_v \frac{\partial}{\partial t}\{\mu^\sigma H\} dv \\ &= n_s\{l_c\}^T \frac{\partial}{\partial t} \int_v \{\mu^\sigma H\} dv \end{aligned} \tag{3.33}$$

Substituting $\{H_e\}$ from Equation-(3.25) in the above equation it can be written as

$$\begin{aligned} V &= -n_s\{l_c\}^T\left[\int_v \{\mu^\sigma[N_H]\}dv\right] \quad [K_{HH}]^{-1}[K_{UH}]^T\frac{\partial}{\partial t}\{U^e\} \\ &= \{F_v\}^T\{\dot{U}^e\} \end{aligned} \tag{3.34}$$

where $\{F_v\}^T$ is

$$\{F_v\}^T = -n_s\{l_c\}^T\left[\int_v \{\mu^\sigma[N_H]\}dv\right] \quad [K_{HH}]^{-1}[K_{UH}]^T. \tag{3.35}$$

3.4 Numerical Experiments

The goal of the analysis is to bring out the effect of coupling on the overall response of 1-D and 2-D composite structures. Hence, for most of the analysis, the results are compared with the uncoupled model to see the effect of coupling. Here we consider four examples of one and two dimensional structures. The first is 1-D magnetostrictive rod model, the second is a composite beam model based on first order shear deformation theory. The third and fourth examples considered plate elements and 2D plane stress/strain elements, respectively. Figure-3.1 shows the various finite elements, with nodes and degrees of freedom. For these examples, static, frequency response and time history analysis are performed to bring out the importance of coupled analysis in the context of structural health monitoring.

3.4.1 Axial Deformation in a Magnetostrictive Rod

To demonstrate the effect of coupling, the above 3-D Equations-(3.24,3.25) reduced to simple 1-D model with mechanical displacement field (u, v, w) as

$$u(x, y, z, t) = u(x); \qquad v = 0; \qquad w = 0 \tag{3.36}$$

and magnetic field H can be reduced as

$$H_x(x, y, z, t) = H(x); \quad H_y(x, y, z, t) = 0; \quad H_z(x, y, z, t) = 0. \tag{3.37}$$

Here, a magnetostrictive rod of length L, cross sectional area A, modulus of Elasticity E, magneto-mechanical strain coefficient d and constant stress permeability μ^σ is considered. For finite element formulation, we use the conventional interpolation function that is,

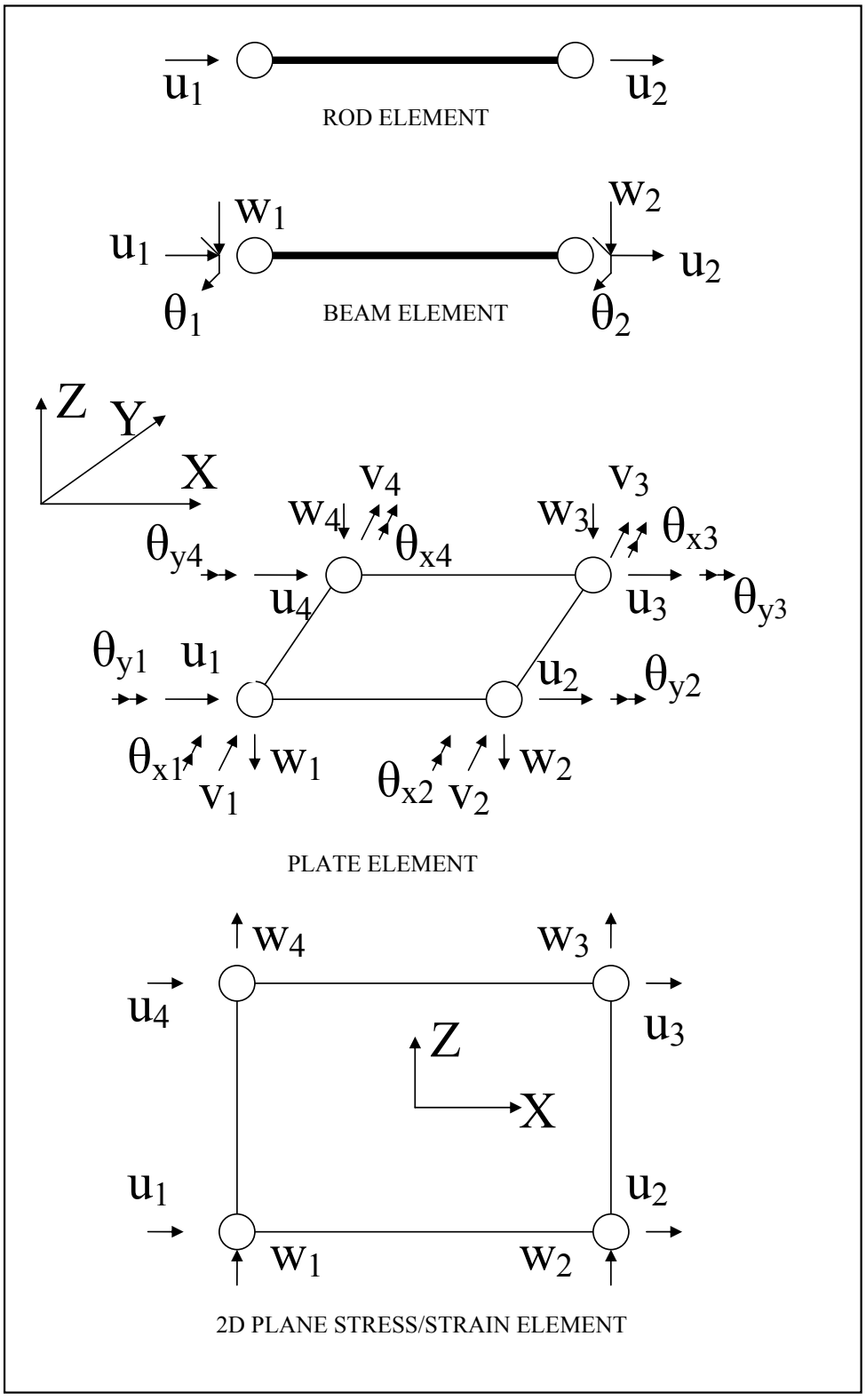

Figure 3.1: Various elements with node and degrees of freedom.

$u(x) = a_0 + a_1 x$, which gives two shape functions as $N_1 = [1 - x/L]$ and $N_2 = [x/L]$. Hence, the displacement field can be written as

$$u(x) = N_1(x)u_1 + N_2(x)u_2 \qquad H(x) = N_1(x)H_1 + N_2(x)H_2 \tag{3.38}$$

Where u_1, u_2 are the element nodal displacement and H_1, H_2 are nodal magnetic fields. Hence, both mechanical and magnetic shape function can be written in matrix form as

$$[N_U] = [N_H] = \begin{bmatrix} 1 - \dfrac{x}{L} & \dfrac{x}{L} \end{bmatrix} \tag{3.39}$$

Using Equation-(3.5), the strain-displacement matrix can be written as

$$\bar{B} = \begin{bmatrix} -\dfrac{1}{L} & \dfrac{1}{L} \end{bmatrix} \tag{3.40}$$

where strain $\epsilon = \frac{\partial u}{\partial x}$. Using Equations-(3.13) and (3.10), the mass matrix $[M_{UU}]$, the stiffness matrix $[K_{UU}]$ and coupling matrix $[K_{UH}]$, can be calculated as

$$\begin{aligned} [M_{UU}] &= \frac{AL\rho}{6} \begin{bmatrix} 2 & 1 \\ 1 & 2 \end{bmatrix}, \\ [K_{UU}] &= \frac{AE}{L} \begin{bmatrix} 1 & -1 \\ -1 & 1 \end{bmatrix}, \\ [K_{UH}] &= \frac{AdE}{2} \begin{bmatrix} -1 & -1 \\ 1 & 1 \end{bmatrix}. \end{aligned} \tag{3.41}$$

The matrix $[K_{HH}]$ can be calculated from Equation-(3.16) as

$$[K_{HH}] = \frac{AL\mu^{\epsilon}}{6} \begin{bmatrix} 2 & 1 \\ 1 & 2 \end{bmatrix} \tag{3.42}$$

The force vector $\{F_H\}$ can be calculated from Equation-(3.19) as

$$\{F_H\} = \frac{I\mu^{\sigma} ALn}{2} \begin{bmatrix} 1 \\ 1 \end{bmatrix} \tag{3.43}$$

Now, using these matrices, we can perform both coupled and uncoupled static analysis.

3.4.1.1 Uncoupled Analysis

For static uncoupled analysis, the corresponding equations become

$$\frac{AE}{L} \begin{bmatrix} 1 & -1 \\ -1 & 1 \end{bmatrix} \begin{bmatrix} u_1 \\ u_2 \end{bmatrix} - \frac{AdE}{2} \begin{bmatrix} -1 & -1 \\ 1 & 1 \end{bmatrix} \begin{bmatrix} H_1 \\ H_2 \end{bmatrix} = \begin{bmatrix} R_1 \\ R_2 \end{bmatrix} \tag{3.44}$$

Where u_1 & u_2 are the two nodal axial displacements in a magnetostrictive rod. $H_1 = H_2 = nI$ as per Equation-(3.21) considering $k_c = n$. Here, we considered three cases for uncoupled analysis

1) Keeping mechanically fixed boundary condition, $u_1 = u_2 = \epsilon = 0$, the blocked force in the fixed support and the stress becomes

$$R_1 = -R_2 = AdEH_1 = AdEIn, \qquad \sigma = dEIn. \tag{3.45}$$

2) For mechanically free boundary condition, where $R_1 = R_2 = \sigma = 0$ ($u_1 = 0$ to remove rigid body displacement).

$$u_2 = LdnI, \qquad \epsilon = dnI. \tag{3.46}$$

3) If the coil current is zero (usually for sensors), we have $H_1 = H_2 = 0$. If a constant tensile force acts and if $u_1 = 0$ (to remove rigid body displacement), then $u_2 = \frac{FL}{AE}$, which is the conventional strength of material solution. Stress $\sigma = \frac{F}{A}$, which satisfies equilibrium equation. Magnetic flux density, which will be used for sensing can be written as:

$$B = \frac{dEu_2}{L} = \frac{dF}{A} = d\sigma = e\epsilon. \tag{3.47}$$

Now, the same set of analysis is performed using coupled model to see the essential differences in the response.

3.4.1.2 Coupled Analysis

For static coupled analysis, corresponding equations are

$$\frac{AE}{L}\begin{bmatrix} 1 & -1 \\ -1 & 1 \end{bmatrix}\begin{bmatrix} u_1 \\ u_2 \end{bmatrix} - \frac{AdE}{2}\begin{bmatrix} -1 & -1 \\ 1 & 1 \end{bmatrix}\begin{bmatrix} H_1 \\ H_2 \end{bmatrix} = \begin{bmatrix} R_1 \\ R_2 \end{bmatrix} \tag{3.48}$$

$$\frac{AdE}{2}\begin{bmatrix} -1 & 1 \\ -1 & 1 \end{bmatrix}\begin{bmatrix} u_1 \\ u_2 \end{bmatrix} + \frac{AL\mu^{\epsilon}}{6}\begin{bmatrix} 2 & 1 \\ 1 & 2 \end{bmatrix}\begin{bmatrix} H_1 \\ H_2 \end{bmatrix} = \frac{I\mu^{\sigma}ALn}{2}\begin{bmatrix} 1 \\ 1 \end{bmatrix} \tag{3.49}$$

The same three cases are considered here

1) Keeping mechanically fixed boundary condition, $u_1 = u_2 = \epsilon = 0$, Equation-(3.49) is solved to obtain the nodal magnetic field, which is given by

$$H_1 = H_2 = In\frac{\mu^{\sigma}}{\mu^{\epsilon}} \tag{3.50}$$

The value of magnetic field is more than the generally considered value (In) for uncoupled model. The value of magnetic field will increase (decrease) with the

increase (decrease) in the ratio of $\frac{\mu^\sigma}{\mu^\epsilon}$. Similarly the blocked force in the support is obtained from Equation-(3.48) and is given by

$$R_1 = -R_2 = AdEH_1 = AdEIn\frac{\mu^\sigma}{\mu^\epsilon} \tag{3.51}$$

which is more than the value generally considered ($AdEIn$). This also depends on the ratio of permeabilities.

2) For mechanically free boundary condition, where $R_1 = R_2 = 0$ ($u_1 = 0$ to remove rigid body displacement), the Equations (3.48-3.49) are solved to obtain.

$$H_1 = H_2 = H = In \quad u_2 = LdnI \quad \epsilon = dnI \tag{3.52}$$

That is $H = In$ is only true for a free-free boundary conditions. For the other boundary conditions, the magnitude of magnetic field depends on the ratio of permeabilities. Stress $\sigma = E\frac{u_2}{L} - EdH = 0$ which satisfies equilibrium equation of free rod at mechanically free boundary condition.

3) For a sensor with tensile force F and zero coil current ($I = 0$), where $-R_1 = R_2 = F$ ($u_1 = 0$ to remove rigid body displacement).

$$\begin{aligned} H_1 = H_2 = -\frac{Fd}{A\mu^\sigma} \qquad u_2 = \frac{FL\mu^\epsilon}{AE\mu^\sigma} \\ B = e\epsilon + \mu^\sigma H = 0 \Rightarrow e\epsilon = -H\mu^\sigma \end{aligned} \tag{3.53}$$

Hence again the dependence on the ratio of permeabilities is very important. Stress $\sigma = E\epsilon - eH = \frac{F}{A}$ which satisfies equilibrium equation.

Hence, It is clear that due to coupling, magnetic field and hence blocked force of a mechanically fixed rod is less than the value generally considered in uncoupled model. The ratio between these two values is calculated for Terfenol-D rod taking data from Terfenol-D manual [52]. Considering $d = 15E-9$ m/amp, $E = 30$ GPa and constant stress relative permeability equal to 10, $\frac{\mu^\sigma}{\mu^\epsilon} = 0.46$, which is around 50% of the value generally considered. However, for any other material, if $\mu^\epsilon \gg d^2E$, then $\mu^\sigma \approx \mu^\epsilon$ and uncoupled and coupled model will give similar result. But for giant magnetostrictive materials like Terfenol-D, the effect of coupling stiffness matrix is considerable on the axial response.

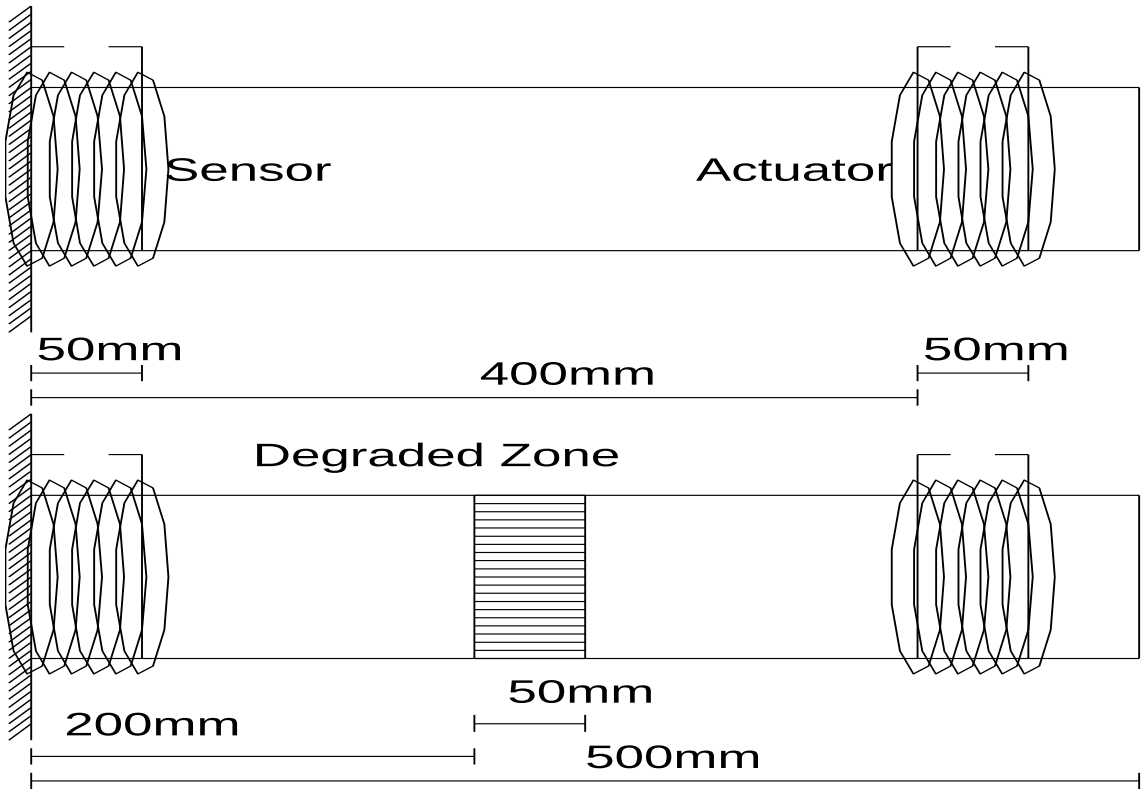

Figure 3.2: Composite Rod With Magnetostrictive Sensor and Actuator

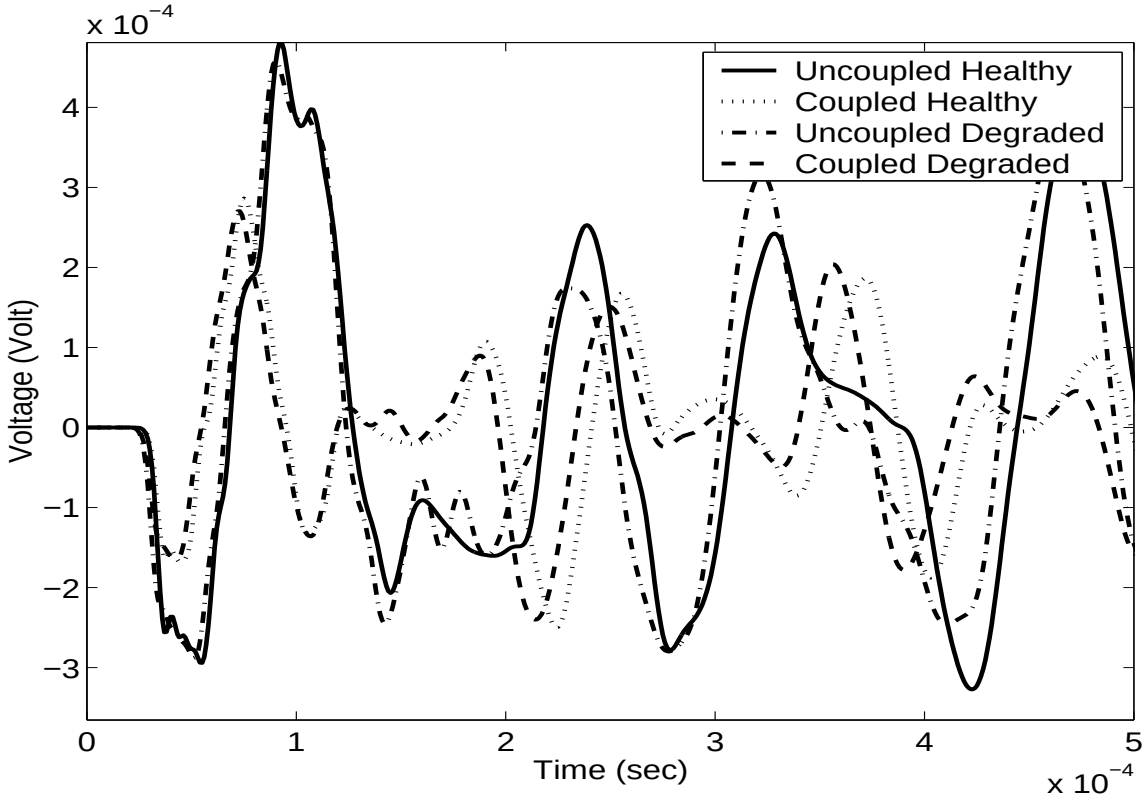

Figure 3.3: Open Circuit Voltages at Magnetostrictive Sensor

3.4.1.3 Degraded Composite Rod with Magnetostrictive Sensor/Actuator

Figure-3.2 shows a composite rod with two magnetostrictive zones, one for actuator and other for sensor. Between the sensor and actuator location, a small degraded zone of 50 mm dimension is placed. Length of the rod is assumed as 500 mm. Cross sectional area of the rod is $90mm^2$. 50mm long sensor is placed near the support. Actuator of length 50mm is at 400mm apart from support. 200 turns of coils are used in both sensing and actuation coils. Magnetostrictive actuator is elongated by 5 kHz frequency current (see Figure-3.6(b)) and magnetostrictive sensor is used to sense the stress wave through the sensing coil. For the case, when a part of a long composite rod is exposed to chemical reaction, elastic property of the structure will degrade. This technique can be used to identify the material degradation zone in the rod. In addition, any change of cross-sectional area from 10% and up can be identified in rod model, which can be a very cost effective technique for long-range composite piping inspection.

Figure-3.3 shows the open circuit voltages in the sensor for coupled, uncoupled, healthy and degraded beam. The degraded zone is modelled by reducing the elastic properties by 10%. This figure shows that there is a significant difference in the response between the coupled and uncoupled responses for both healthy and degraded case. However, the responses for healthy and degraded case vary only marginally at higher time steps. This is expected since only 10% of the property is degraded. This example clearly shows the need for coupled formulation.

3.4.2 Finite Element Formulation for a Beam

In this subsection, a shear deformable Finite Element (FE) is deduced from the 3-D FE formulation. In particular, the effect of stiffness coupling is brought out on the static and dynamic responses. Mechanical displacement fields are considered as

$$u(x,y,z,t) = u^0(x,t) - z\theta_x^0(x,t), \quad v(x,y,z,t) = 0, \quad w(x,y,z,t) = w^0(x,t). \quad (3.54)$$

Where u, v, w are the components of mechanical displacement at location (x, y, z) in X, Y and Z direction (see Figure-3.4) respectively. u^0 and w^0 are the displacement components in mid plane of the composite beam. θ_x^0 is the slope of the mid plane about X axis. Magnetic fields in three coordinate directions are

$$H_x(x,y,z,t) = H_{xp}^0(x,t), \quad H_y(x,y,z,t) = 0, \quad H_z(x,y,z,t) = 0. \quad (3.55)$$

H^0_{xp} is X directional magnetic field at mid plane of the magnetostrictive patch p. The magnetic field along the thickness direction within a particular layer is assumed as constant. In matrix notation, Equation-(3.54) can be written as

$$\{U\} = \begin{Bmatrix} u \\ v \\ w \end{Bmatrix} = \begin{bmatrix} 1 & 0 & -z \\ 0 & 0 & 0 \\ 0 & 1 & 0 \end{bmatrix} \begin{Bmatrix} u^0 \\ w^0 \\ \theta^0 \end{Bmatrix} = [N_p]\{\bar{U}\} \tag{3.56}$$

For finite element formulation, displacement and magnetic fields are discretized as

$$\begin{aligned} u^0(x) &= N_1(x)u_1 + N_2(x)u_2 \qquad & w^0(x) &= N_1(x)w_1 + N_2(x)w_2 \\ \theta^0(x) &= N_1(x)\theta_1 + N_2(x)\theta_2 \qquad & H(x) &= N_1(x)H_1 + N_2(x)H_2 \end{aligned} \tag{3.57}$$

That is each node has four degrees of freedom. Here u_1, u_2, w_1, w_2, θ_1, θ_2 are the element nodal displacements and slopes and H_1, H_2 are nodal magnetic fields. Equation-(3.57) can be written in matrix form as

$$\{\bar{U}\} = [\bar{N}_U]\{U^e\} \qquad \{H\} = [N_H]\{H^e\}. \tag{3.58}$$

Here, nodal mechanical displacement vector, $\{U^e\}$ and magnetic field vector $\{H^e\}$ are given by

$$\{U^e\} = \{u_1 \;\; w_1 \;\; \theta_1 \;\; u_2 \;\; w_2 \;\; \theta_2\}^T, \qquad \{H^e\} = \{H_1 \;\; H_2\}^T. \tag{3.59}$$

The mechanical and magnetic shape functions can be written as

$$[\bar{N}_U] = \begin{bmatrix} N_1 & 0 & 0 & N_2 & 0 & 0 \\ 0 & N_1 & 0 & 0 & N_2 & 0 \\ 0 & 0 & N_1 & 0 & 0 & N_2 \end{bmatrix}, \qquad [N_H] = \begin{bmatrix} N_1 & N_2 \end{bmatrix} \tag{3.60}$$

where linear shape functions are assumed, which are given by

$$[N_1] = \left[1 - \frac{x}{L}\right], \qquad [N_2] = \left[\frac{x}{L}\right] \tag{3.61}$$

To formulate mechanical shape function, mechanical displacement $\{U\}$ can be written using Equation-(3.56) as

$$\{U\} = [N_p][\bar{N}_U]\{U^e\} = [N_U]\{U^e\} \tag{3.62}$$

where mechanical shape function $[N_U]$ is

$$[N_U] \;=\; \begin{bmatrix} N_1 & 0 & -zN_1 & N_2 & 0 & -zN_2 \\ 0 & 0 & 0 & 0 & 0 & 0 \\ 0 & N_1 & 0 & 0 & N_2 & 0 \end{bmatrix} \tag{3.63}$$

The strain displacement matrix $[\bar{B}]$ can be written from Equation-(3.5) as follows

$$[\bar{B}] = [\mathcal{L}][N_U] = \begin{bmatrix} N_{1,x} & 0 & -zN_{1,x} & N_{2,x} & 0 & -zN_{2,x} \\ 0 & 0 & 0 & 0 & 0 & 0 \\ 0 & 0 & 0 & 0 & 0 & 0 \\ 0 & 0 & 0 & 0 & 0 & 0 \\ 0 & N_{1,x} & -N_1 & 0 & N_{2,x} & -N_2 \\ 0 & 0 & 0 & 0 & 0 & 0 \end{bmatrix} \tag{3.64}$$

The stiffness matrix $[K_{UU}]$ can be calculated from Equation-(3.10). To avoid shear locking, shear part of the $[K_{UU}]$ matrix is reduced integrated. Values of nonzero elements of stiffness matrix $[K_{UU}]$ of a composite laminated beam are the following

$$K_{11} = \frac{A_{11}}{L}, \quad K_{12} = \frac{A_{15}}{L}, \quad K_{13} = \frac{A_{15}}{2} - \frac{B_{11}}{L}, \quad K_{14} = -\frac{A_{11}}{L},$$

$$K_{15} = -\frac{A_{15}}{L}, \quad K_{16} = \frac{A_{15}}{2} + \frac{B_{11}}{L}, \quad K_{22} = \frac{A_{55}}{L}, \quad K_{23} = \frac{A_{55}}{2} - \frac{B_{15}}{L},$$

$$K_{24} = -\frac{A_{15}}{L}, \quad K_{25} = -\frac{A_{55}}{L}, \quad K_{26} = \frac{A_{55}}{2} + \frac{B_{15}}{L},$$

$$K_{33} = \frac{A_{55}L}{4} - B_{15} + \frac{D_{11}}{L}, \quad K_{34} = -\frac{A_{15}}{2} + \frac{B_{11}}{L},$$

$$K_{35} = -\frac{A_{55}}{2} + \frac{B_{15}}{L}, \quad K_{36} = \frac{A_{55}L}{4} - \frac{D_{11}}{L}, \quad K_{44} = \frac{A_{11}}{L}, \quad K_{45} = \frac{A_{15}}{L},$$

$$K_{46} = -\frac{A_{15}}{2} - \frac{B_{11}}{L}, \quad K_{55} = \frac{A_{55}}{L},$$

$$K_{56} = -\frac{A_{55}}{2} - \frac{B_{15}}{L}, \quad K_{66} = \frac{A_{55}L}{4} + B_{15} + \frac{D_{11}}{L},$$

$$K_{ij} = K_{ji} \quad [\, i, j = 1 \; to \; 6].$$

where A_{ij}, B_{ij}, D_{ij} are

$$[A_{ij} \;\; B_{ij} \;\; D_{ij}] = \int \bar{Q}_{ij}[1 \;\; z \;\; z^2]dA \tag{3.65}$$

The mass matrix $[M_{UU}]$ can be calculated from Equation-(3.13) and is given by

$$[M_{UU}] = \frac{L}{6}\begin{bmatrix} 2I_0 & 0 & -2I_1 & I_0 & 0 & -I_1 \\ 0 & 2I_0 & 0 & 0 & I_0 & 0 \\ -2I_0 & 0 & 2I_2 & -I_1 & 0 & I_2 \\ I_0 & 0 & -I_1 & 2I_0 & 0 & -2I_1 \\ 0 & I_0 & 0 & 0 & 2I_0 & 0 \\ -I_1 & 0 & I_2 & -2I_1 & 0 & 2I_2 \end{bmatrix}. \tag{3.66}$$

where I_0, I_1, I_2 are the mass, first moment of mass and second moment of mass per unit length of the beam and are given by

$$[I_0 \;\; I_1 \;\; I_2] = \int_A \rho[1 \;\; z \;\; z^2]dA \tag{3.67}$$

The matrix $[e]$ in Equations-(2.9) & (2.10) for beam element takes the form as

$$[e] = \begin{bmatrix} e_{11} & 0 & 0 & 0 & 0 & 0 \end{bmatrix} \tag{3.68}$$

since the magneto-mechanical stress will be experienced only in the axial direction due to beam bending. The matrix $[K_{UH}]$ can be calculated from Equation-(3.10) as

$$[K_{UH}]^T = \frac{1}{2}\begin{bmatrix} -e_{11}^0 & 0 & e_{11}^1 & e_{11}^0 & 0 & -e_{11}^1 \\ -e_{11}^0 & 0 & e_{11}^1 & e_{11}^0 & 0 & -e_{11}^1 \end{bmatrix} \tag{3.69}$$

Where e_{11}^0 and e_{11}^1 are given by

$$\begin{bmatrix} e_{11}^0 & e_{11}^1 \end{bmatrix} = \int_A e_{11}\begin{bmatrix} 1 & z \end{bmatrix} dA \tag{3.70}$$

The matrix $[K_{HH}]$ can be calculated from Equation-(3.16) as

$$[K_{HH}] = \frac{L\mu^0}{6}\begin{bmatrix} 2 & 1 \\ 1 & 2 \end{bmatrix} \tag{3.71}$$

Where μ^0 is

$$[\mu^0] = \int_A \mu^\epsilon dA \tag{3.72}$$

$\{F_H\}$ and $\{F_v\}$ from Equations-(3.19), (3.31) and (3.35) can be written as

$$\begin{aligned} \{F_H\}^T &= \frac{In\mu^0 L}{2}\begin{bmatrix} 1 & 1 \end{bmatrix}, \\ \{F_v\}^T_{Unoupled} &= n\begin{bmatrix} e_{11}^0 & 0 & -e_{11}^1 & -e_{11}^0 & 0 & e_{11}^1 \end{bmatrix}, \\ \{F_v\}^T_{Coupled} &= n\begin{bmatrix} e_{11}^{0r} & 0 & -e_{11}^{1r} & -e_{11}^{0r} & 0 & e_{11}^{1r} \end{bmatrix}. \end{aligned} \tag{3.73}$$

Where e_{11}^{0r} and e_{11}^{1r} are given

$$\begin{bmatrix} e_{11}^{0r} & e_{11}^{1r} \end{bmatrix} = \int_A e_{11} \frac{\mu^\sigma}{\mu^\epsilon} \begin{bmatrix} 1 & z \end{bmatrix} dA \tag{3.74}$$

3.4.2.1 Composite Beam with Magnetostrictive Bimorph

Numerical simulation is carried out by considering a laminated composite beam of total thickness 1.8mm as shown in Figure-3.4. Length and width of the beam is 500mm and 50mm respectively. The beam is made of 12 layers with thickness of each layer being 0.15 mm. Surface mounted magnetostrictive patches at the top and bottom layer are considered as sensor and actuator, respectively. Elastic modulus of composite is assumed

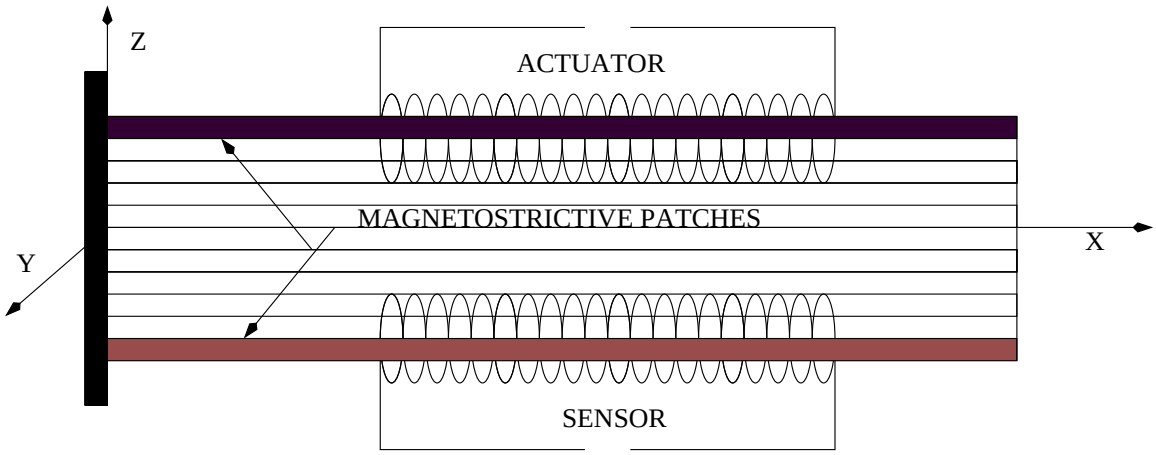

Figure 3.4: Laminated Beam With Magnetostrictive Patches.

as 181 GPa and 10.3 GPa, in the parallel (E_1) and the perpendicular (E_2) direction of fiber. Poisson's ratio (ν), density (ρ) and shear modulus (G_{12}) of composite are assumed as 0.0, 1.6 gm/c.c. and 28 GPa, respectively. Elastic modulus (E_m), poisson's ratio (ν_m), shear modulus (G_m) and density (ρ_m) of the magnetostrictive material are taken as 30 GPa, 0.0, 23 GPa and 9.25 gm/c.c. respectively. Magneto-mechanical coupling coefficient is taken as 15E-09 m/amp. Permeability at vacuum or air is assumed to be 400 π nano-Henry/m. Constant stress relative permeability of magnetostrictive material is considered as 10. Number of coil turn per meter (n) in sensor and actuator is assumed to be 20000. Three different analyses, namely the static, the frequency response and the time history analysis are performed to bring out the essential difference in the responses between coupled and uncoupled models.

3.4.2.2 Static Analysis

Table 3.1: Vertical Displacement of Cantilever Tip

Ply Sequence	Coupled w_c mm	Uncoupled w_u mm	Ratio w_u/w_c
$m/[0]_{10}/m$	2.17	2.44	1.12
$m/[30]_{10}/m$	2.83	3.30	1.17
$m/[45]_{10}/m$	3.84	4.78	1.24
$m/[60]_{10}/m$	5.52	7.69	1.39
$m/[90]_{10}/m$	8.62	15.40	1.78
$m/[0/90]_5/m$	3.44	4.80	1.40
$m/[90/0]_5/m$	7.26	10.73	1.48
$[m]_2/[0]_8/[m]_2$	5.25	6.97	1.33
$[m]_2/[30]_8/[m]_2$	6.03	8.41	1.39
$[m]_2/[45]_8/[m]_2$	7.07	10.58	1.50
$[m]_2/[60]_8/[m]_2$	8.53	14.22	1.68
$[m]_2/[90]_8/[m]_2$	10.72	21.56	2.01
$[m]_2/[0]_4/[90]_4/[m]_2$	6.23	10.34	1.66
$[m]_2/[90]_4/[0]_4/[m]_2$	10.77	19.57	1.82
$[m]_3/[0]_6/[m]_3$	8.88	14.39	1.62
$[m]_3/[30]_6/[m]_3$	9.20	15.00	1.63
$[m]_3/[45]_6/[m]_3$	9.62	16.50	1.72
$[m]_3/[60]_6/[m]_3$	10.56	19.40	1.84
$[m]_3/[90]_6/[m]_3$	12.15	25.53	2.10
$[m]_3/[0]_3/[90]_3/[m]_3$	9.00	16.60	1.84
$[m]_3/[90]_3/[0]_3/[m]_3$	12.88	26.31	2.04
$[m]_4/[0]_4/[m]_4$	12.08	23.41	1.93
$[m]_4/[30]_4/[m]_4$	11.48	21.24	1.85
$[m]_4/[45]_4/[m]_4$	11.45	21.15	1.85
$[m]_4/[60]_4/[m]_4$	12.00	23.10	1.93
$[m]_4/[90]_4/[m]_4$	13.3	28.47	2.14
$[m]_4/[0]_2/[90]_2/[m]_4$	11.62	23.10	1.99
$[m]_4/[90]_2/[0]_2/[m]_4$	14.06	30.44	2.17

The effect of coupling of magnetostrictive material in a laminated composite beam for static actuation is analyzed for 1 Amp DC actuation coil current. It is observed that tip deflection for coupled analysis is 2.17mm, where as for uncoupled analysis, it is found to be 2.44mm. The ratio between these two is 1.12. As the thickness of the actuator is less compared to the thickness of the composite beam, the effective increase of stiffness in the global stiffness matrix due to coupling is very less. Increase of thickness of sensor

and actuator patches will increase the effective thickness and hence decrease the effective deflection, especially in the coupled analysis. In addition, increase of ply angle will also increase the stiffness in the transverse direction. This aspect is shown in Table-3.1 for different ply angles range from 0^0 to 90^0. It is very clear from the table that for 90^0 ply angle, the effect of coupling is considerable. This reinforces the need for coupled analysis for structures with magnetostrictive patches. In the next two analyses, the effect of coupling in dynamic analysis in the context of structural health monitoring is further emphasized.

3.4.2.3 Frequency Response Analysis of a Healthy and Delaminated Beam

In the FE modelling, delamination in the composite beam is modelled using two sub-laminates, one for top and other for bottom part of the delamination. Stiffness or mass matrices of the elements for top sub-laminate are integrated from the delaminated layer to the top layer and for the bottom sub-laminate, from the bottom layer to the delaminated layer. FE nodes for top sub-laminate are only connected with the elements for top sub-laminate and similarly, nodes for bottom sub-laminate are connected with the elements for bottom sub-laminate. Physical locations of these two sets of FE nodes are in the neutral axis of the original beam. Hence, two nodes will exist in the delaminated zones, one for elements of top sub-laminate and other for elements of bottom sub-laminate. These two nodes are not directly connected with any element. Detail modelling of delamination is explained in section-6.2 with examples and with Figure-6.1.

To observe the effects of coupling terms of magnetostrictive material in the frequency domain, frequency response function (FRF) is calculated with both coupled and uncoupled model for the same cantilever composite beam up to 3^{rd} natural frequencies. FRF for 0^0 and 90^0 ply angle is shown in Figure-3.5(a) and Figure-3.5(b) respectively. For 0^0 ply angle, we see that the first two modes are least effected due to the effect of coupling. However, we can see significant shift in resonant frequency of higher modes. For the 90^0 ply angle, one sees the shift in the natural frequencies even for first mode. This farther reinforces our belief that uncoupled analysis under estimate the stiffness of the structure with magnetostrictive material. From the structural health monitoring point of view, the difference in the responses between the healthy and the damaged structures indicate the presence of the defect. FRFs for the same beam with 100mm mid layer delamination at 100mm apart from support are also shown in the same figures for both coupled and uncoupled material model. In both the figures, it is observed that, the higher modes

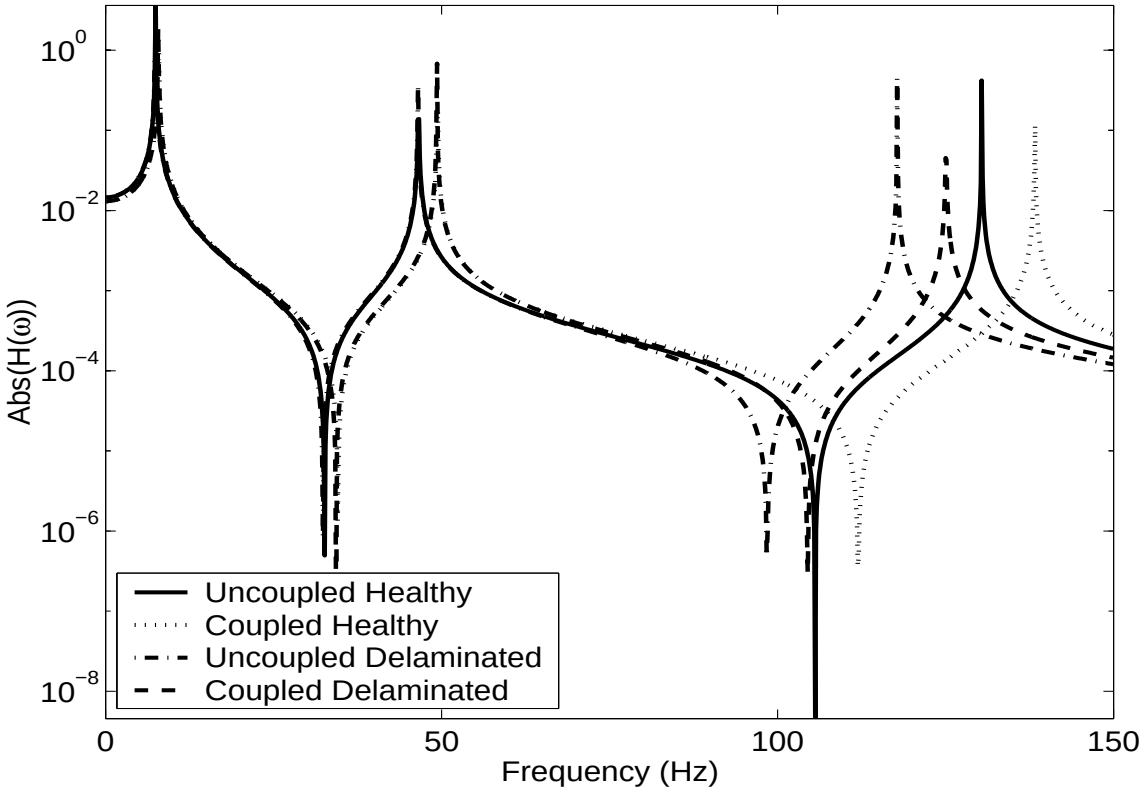

(a) 0^0 ply angle

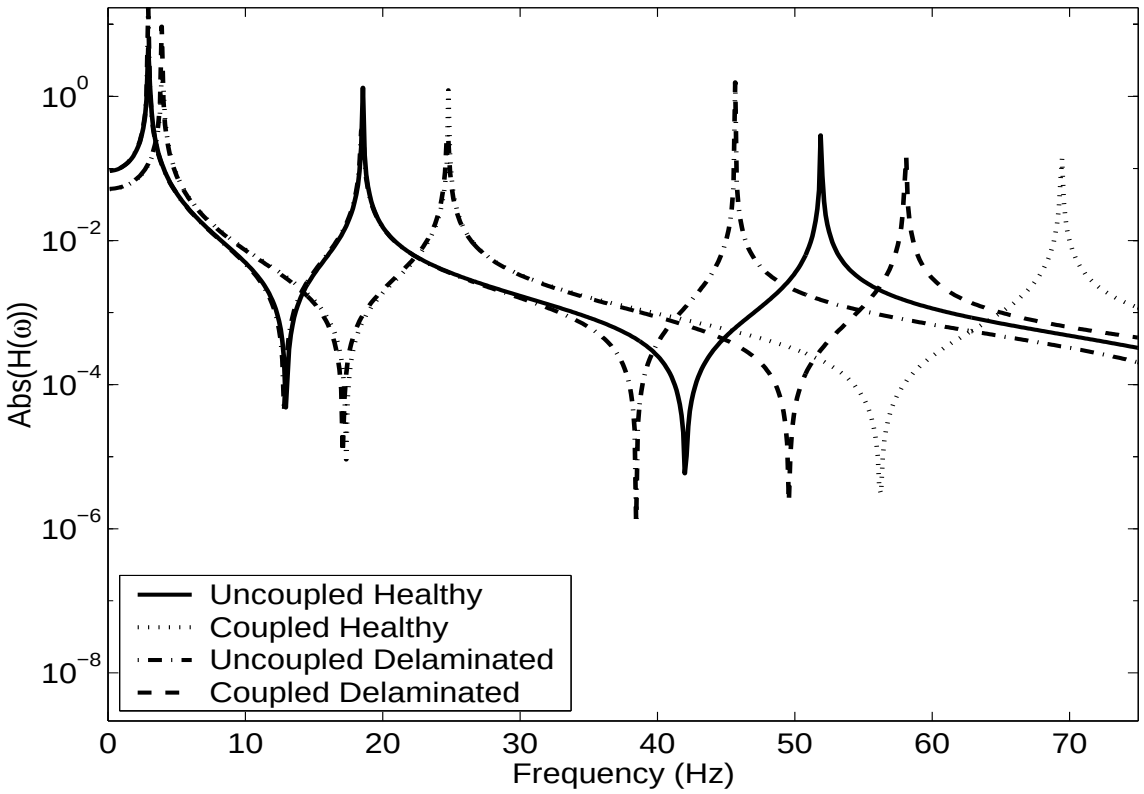

(b) 90^0 ply angle

Figure 3.5: Frequency Response Function

are slightly affected while the initial modes are affected least. In addition, the damage sensitivity in the FRF of the structure is less than the error due to uncoupled assumption of analysis. Yet another parameter where the effect of coupled analysis requires investigation is the frequency of the AC current required to generate the magnetic field. This can be seen from the time history analysis, which is given in next subsection.

3.4.2.4 Time Domain Analysis

To observe the effects of coupled analysis on structure with magnetostrictive material, time domain analysis is carried out for both low and high frequency actuation for the same cantilever composite beam. Here, the structure is actuated through a sinusoidal time signal current, I of 0.5 amp amplitude AC current (I_0) and 0.5 Amp bias current (I_{DC}) at 50 Hz and 5 kHz frequency, respectively. The equation of current is given by

$$I = I_0 sin(\omega t) + I_{DC} \tag{3.75}$$

These are shown in Figure-3.6(a) and Figure-3.6(b) respectively. Direct transient dynamic analysis is performed for 200 time steps to calculate open circuit voltage of the sensor and beam tip velocity. Each time step is 50 mili-seconds and 5 micro-seconds for 50 Hz and 5 kHz actuation, respectively. Figure-3.7(a) and Figure-3.7(b) shows the tip velocity of the cantilever beam for 50 Hz and 5 kHz respectively with 0^0 ply angle. From these figures, we see that the effect of magneto-mechanical coupling is negligible for both low and high actuation frequency. But sensitivity of delamination in the responses is more in high frequency than low frequency actuation. Figure-3.8(a) and Figure-3.8(b) shows the tip velocity of the cantilever beam for 50 Hz and 5 kHz respectively with 90^0 ply angle. However, with 90^0 degree ply angle, we can start seeing the difference in behavior for actuation frequencies 50 Hz and 5kHz. For low frequency actuation, coupling has phenomenal effect. At high frequency actuation, there is no period error. However, coupling introduces lower velocity amplitudes.

Figure-3.7(a) and Figure-3.8(a) show high frequency signal at the start of the response. To avoid double frequency effect in magnetostrictive actuator, windowed sinusoidal current amplitude is biased with DC current, which has both low frequency as well as high frequency component. In addition, open circuit voltages in sensors are proportional to the time derivative of the stress integrated along the length of the sensor. Initial high frequency signals are due to these extra complicacies of the sensing and actuation calculation, when sensor and actuator exists in the same element of the finite element

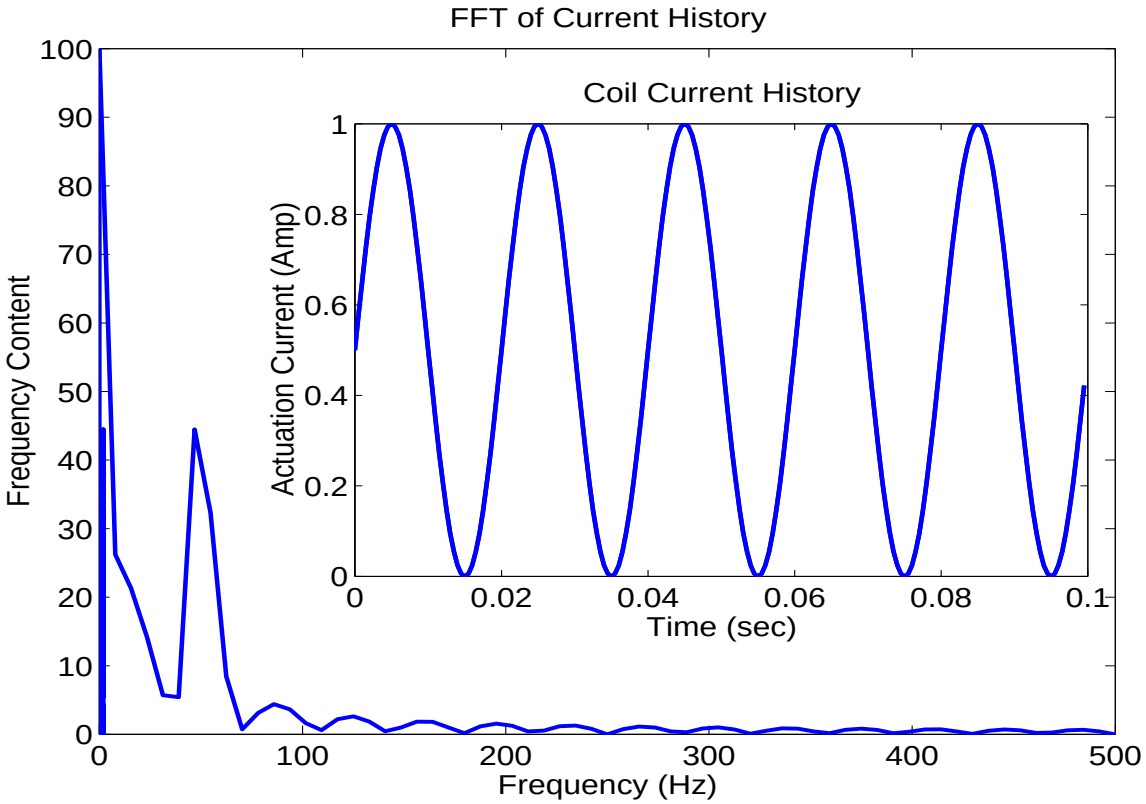

(a) 50Hz Actuation

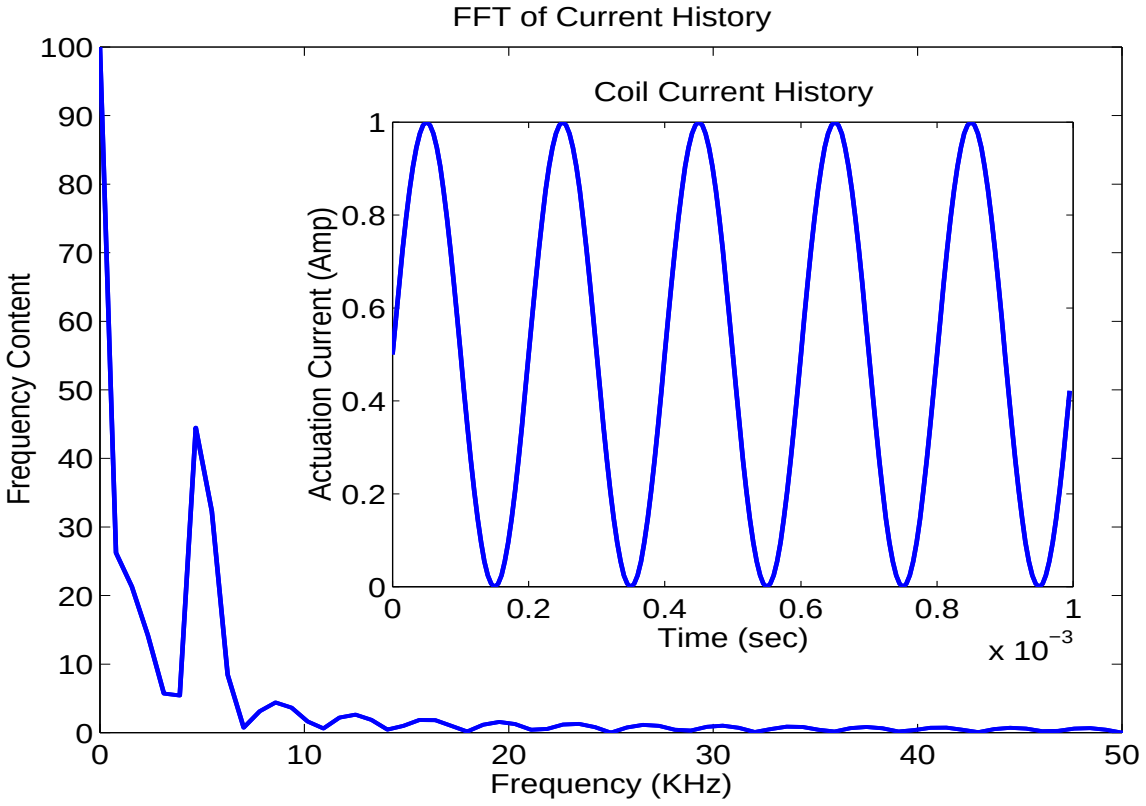

(b) 5 kHz Actuation

Figure 3.6: Actuation History with Frequency content

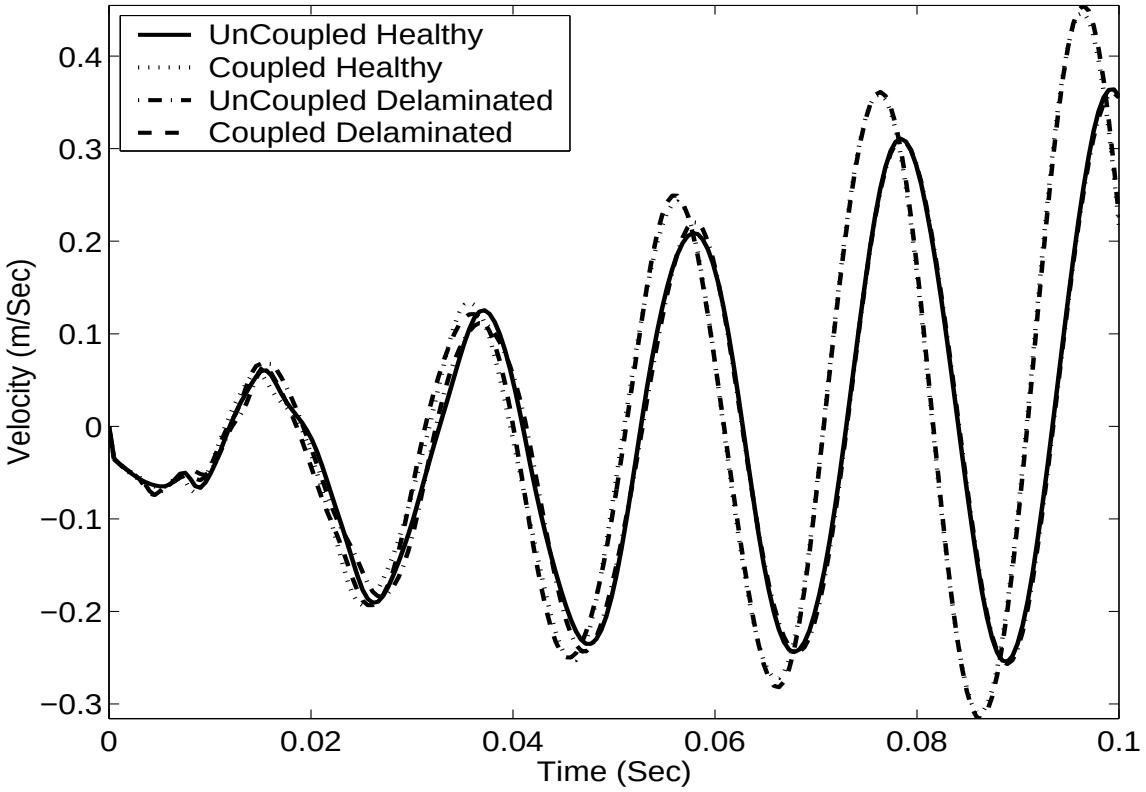

(a) 50Hz Actuation

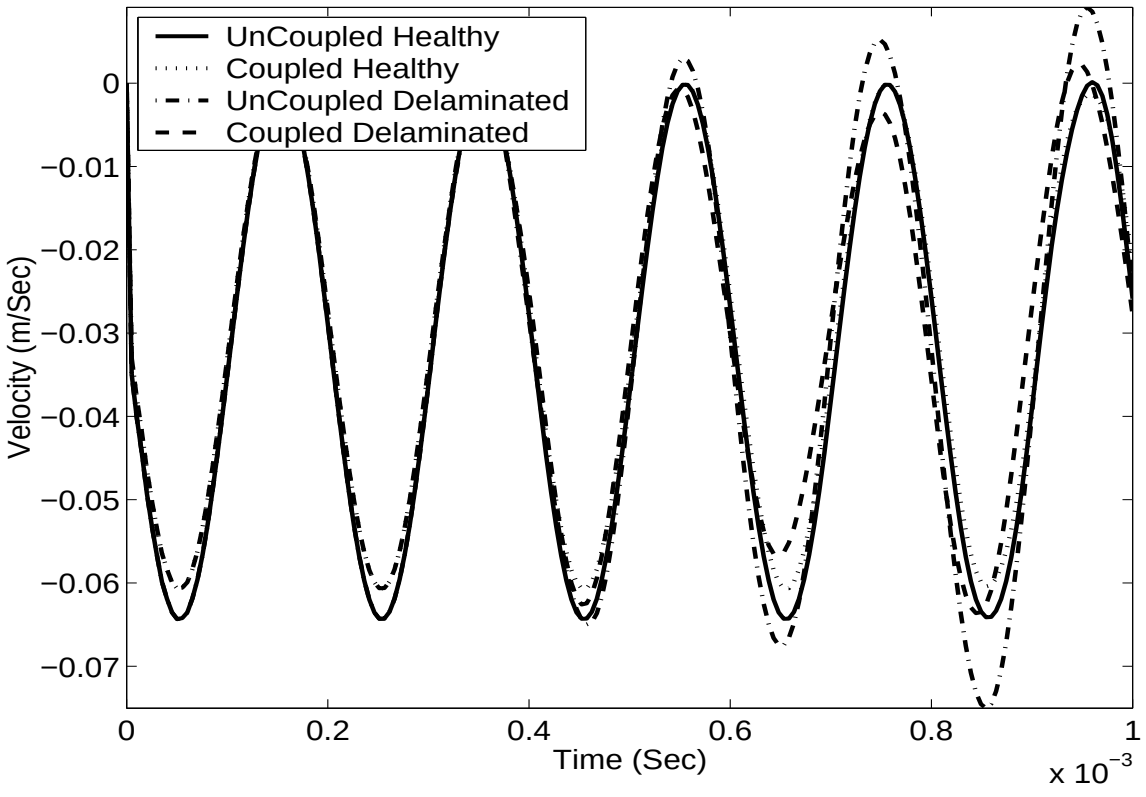

(b) 5 kHz Actuation

Figure 3.7: Cantilever Tip Velocity for 0^0 ply angle

analysis. From the responses of delaminated beam in above figures, it is emphasizing the requirement of coupled analysis for structural health monitoring application.

Figure-3.9(a) and Figure-3.9(b) shows the open circuit voltages generated in the sensory patches for low and high frequency actuating current for 0^0 ply angle laminate. The effect of coupling and damage are almost negligible. However, coupling effect induces significant changes in the voltages for 90^0 ply angle laminate. Figure-3.10(a) shows the open circuit voltages with 90^0 ply angle laminate for 50 Hz actuation. The figure shows that the delamination increases the open circuit voltages in uncoupled analysis, while it decreases in the coupled analysis. Figure-3.10(b) shows the open circuit voltages with 90^0 ply angle for 5 kHz actuation. Differences between the open circuit voltages considering coupled and uncoupled formulation are considerable.

These examples show that the uncoupled model of the laminated composite structure with magnetostrictive patches in most cases gives upper bound solutions, which is highly non-conservative from the structural design point of view. In addition, for structural health monitoring application, the difference in response between the healthy and damaged beam is found significant in the coupled analysis. These studies justify the need for coupled material model for realistic analysis of composite beams with magnetostrictive material patches.

3.4.3 Finite Element Formulation of a Plate

In this subsection, a cantilever plate element with magnetostrictive material patches deduced from the generalized 3-D formulation discussed earlier is studied. The element is based on first order shear deformation theory (Mindlin's theory). Further, this element is used to model a plate with multiple delaminations and the effect of coupled and uncoupled model on the responses of the healthy and delaminated plate is investigated. Mechanical displacement fields can be written as

$$\begin{aligned} u(x,y,z,t) &= u^0(x,y,t) - z\theta_x^0(x,y,t), \\ v(x,y,z,t) &= v^0(x,y,t) - z\theta_y^0(x,y,t), \\ w(x,y,z,t) &= w^0(x,y,t). \end{aligned} \tag{3.76}$$

Where u, v, w are the components of mechanical displacement at location (x, y, z) in X, Y and Z direction respectively. u^0, v^0 and w^0 are the displacement components in mid plane of the composite plate. θ_x^0 and θ_y^0 are the slope of the mid plane about X and Y axis

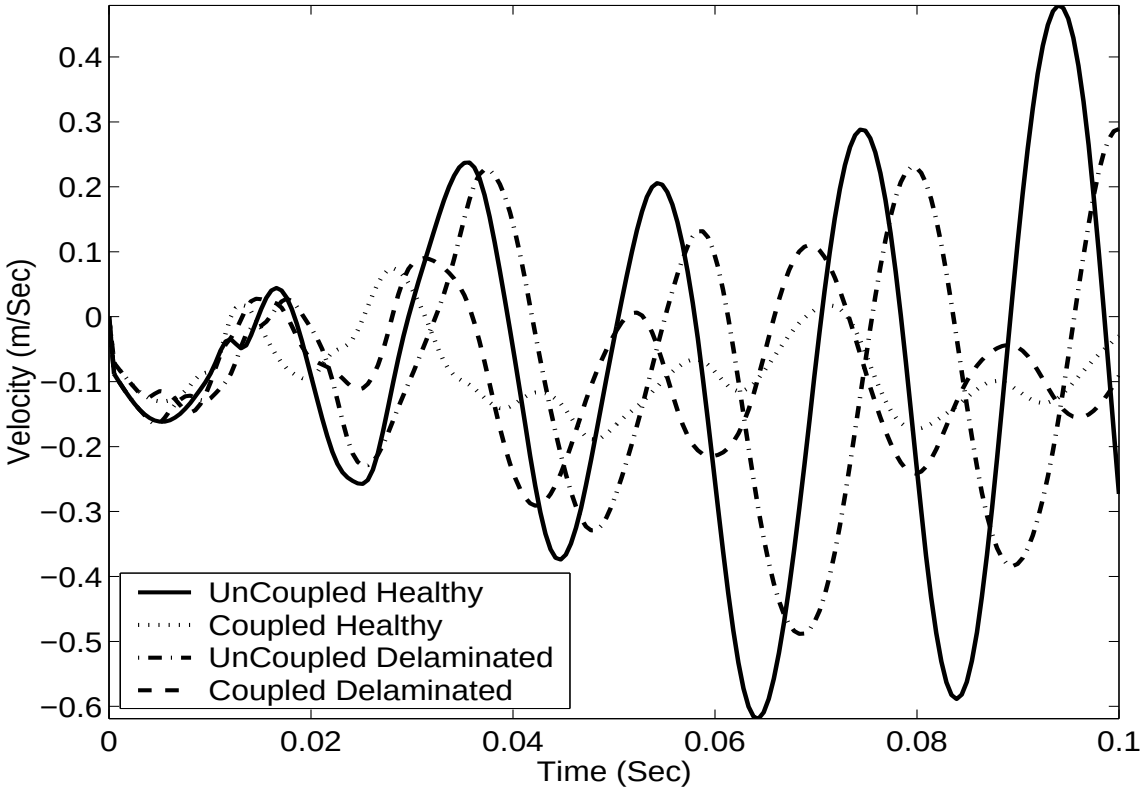

(a) 50Hz Actuation

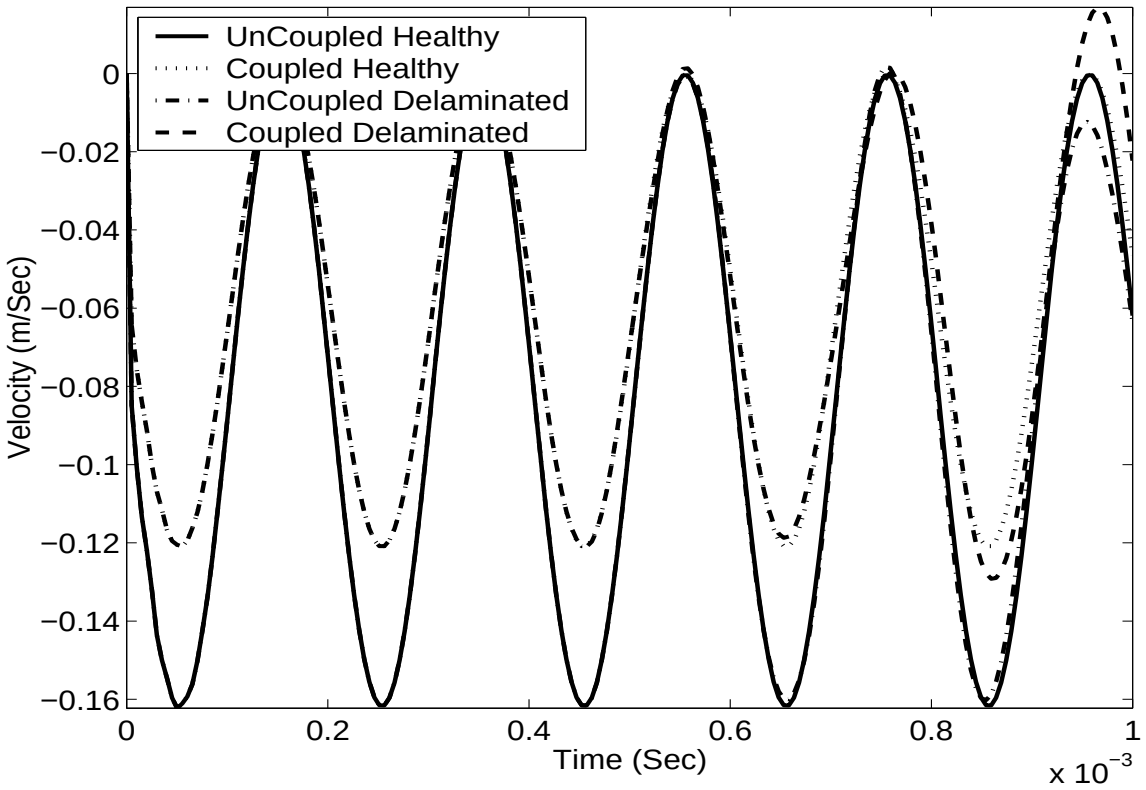

(b) 5 kHz Actuation

Figure 3.8: Cantilever Tip Velocity for 90^0 ply angle.

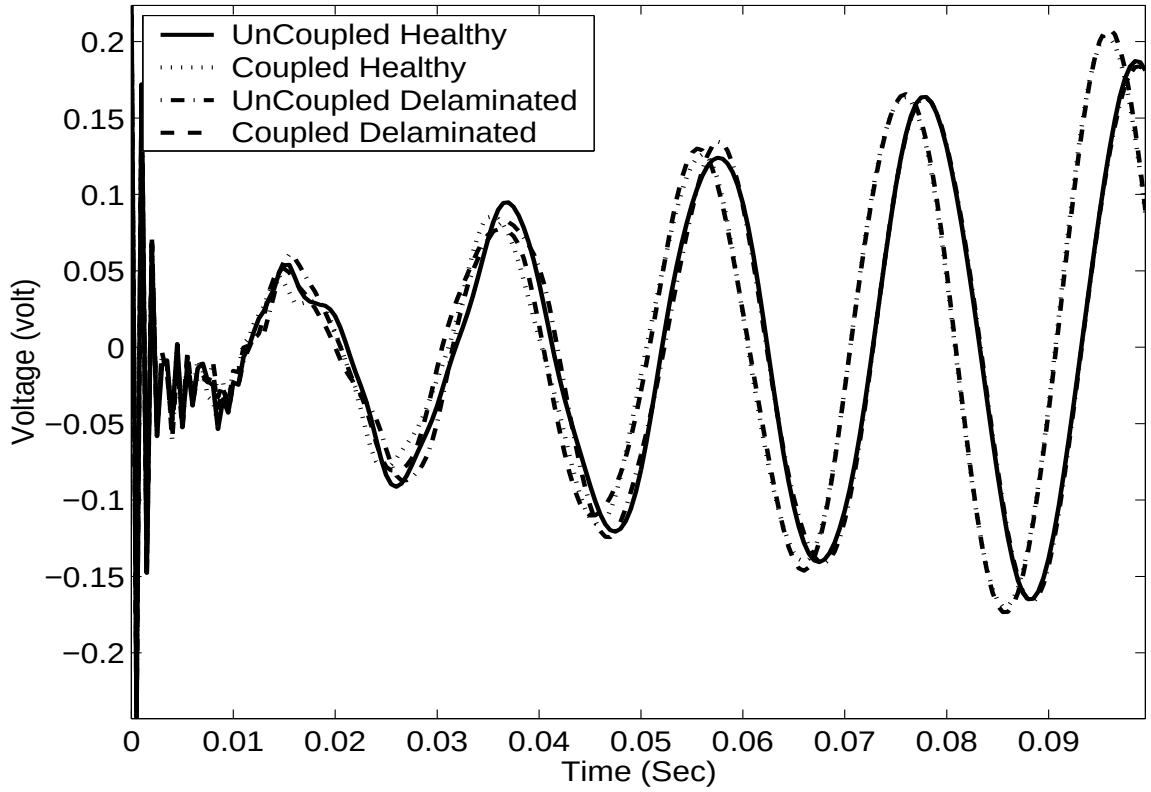

(a) 50Hz Actuation

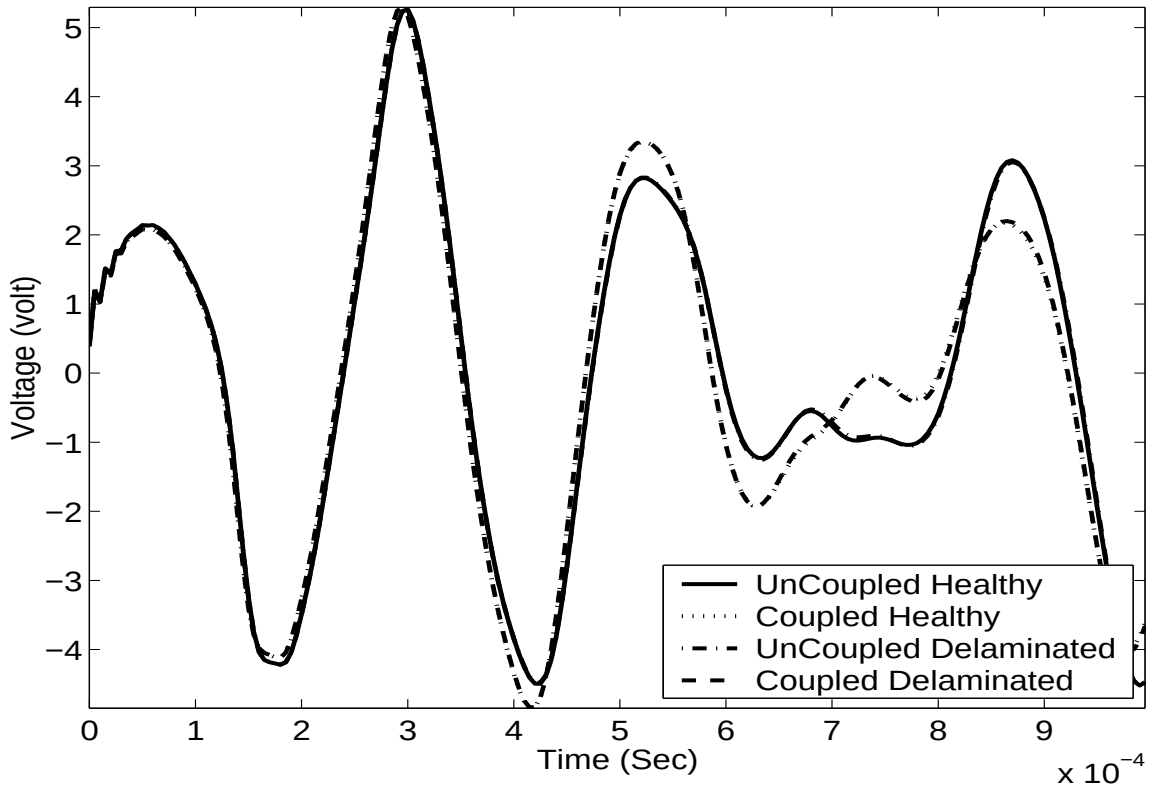

(b) 5 kHz Actuation

Figure 3.9: Sensor Open Circuit Voltage for 0^0 ply angle

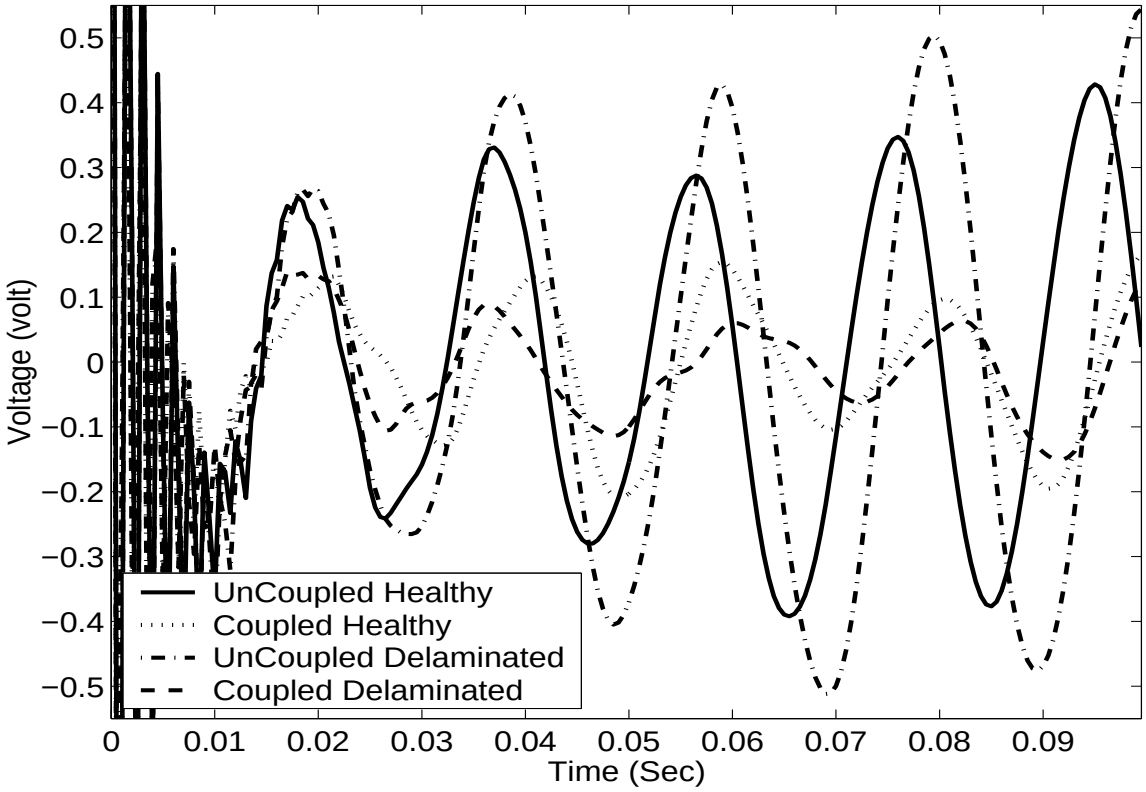

(a) 50Hz Actuation

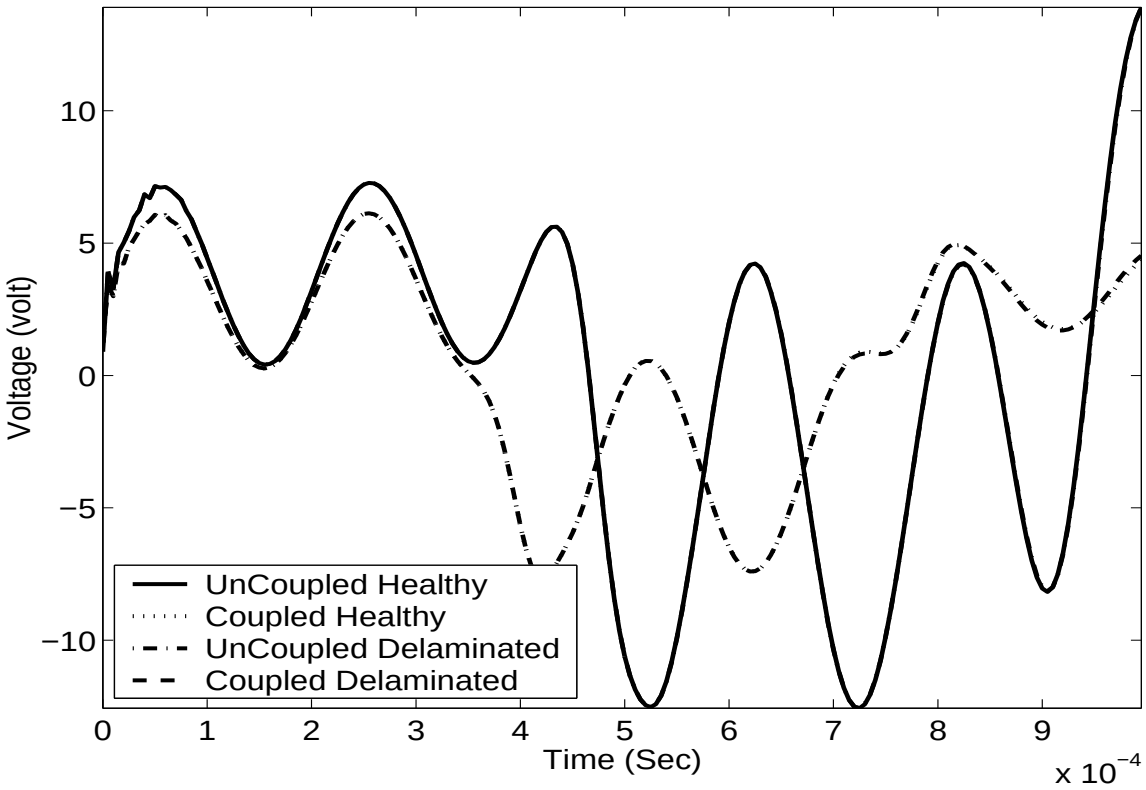

(b) 5 kHz Actuation

Figure 3.10: Sensor Open Circuit Voltage for 90^0 ply angle

respectively. Magnetic fields in three coordinate directions are assumed as

$$H_x(x,y,z,t) = H^0_{xp}(x,y,t), \quad H_y(x,y,z,t) = H^0_{yp}(x,y,t), \quad H_z(x,y,z,t) = 0. \quad (3.77)$$

H^0_{xp} and H^0_{yp} are X and Y directional magnetic field at mid plane of the magnetostrictive patch p respectively. Hence, the magnetic field along the thickness direction within a particular layer is assumed as constant. In matrix notation, Equation-(3.76) can be written as

$$\{U\} = \begin{Bmatrix} u \\ v \\ w \end{Bmatrix} = \begin{bmatrix} 1 & 0 & 0 & -z & 0 \\ 0 & 1 & 0 & 0 & -z \\ 0 & 0 & 1 & 0 & 0 \end{bmatrix} \begin{Bmatrix} u^0 \\ v^0 \\ w^0 \\ \theta^0_x \\ \theta^0_y \end{Bmatrix} = [N_p]\{\bar{U}\} \quad (3.78)$$

Stiffness and mass matrices of plate element are derived using bilinear shape functions with standard 4 noded finite element formulation. Here each node of the element has seven degrees of freedoms (five mechanical and two magnetic degrees of freedom).

Delamination for plate in finite element modelling is performed similar to the beam as discussed in previous section. For single delamination, delaminated zone is modelled with two sets of elements, one for top sub-laminate and other for bottom sub-laminate of the plate. Two sets of nodes are also generated, where only one set is connected with the elements for top sub-laminate and other set is connected with the elements for bottom sub-laminate. Physical location of these nodes are in the neutral plane of the plate, which may differ from the mid plane of these individual sub-laminates. Undelaminated zone is modelled with single set of elements and nodes. These nodes are in the neutral plane of the plate. Interface of the delaminated and undelaminated zone is modelled with merging the nodes, which are physically in the same place. However, two nodes for two sub-laminates and one node for undelaminated laminate are merged in the interface of the delamination for the integrity of the model. For multiple delaminations, similar approach is taken for every delamination one by one in the model. However, where the delaminations are overlapped, more number of sub-laminates are required. Every sub-laminate is modelled with plate elements, where stiffness and mass matrices for these elements are calculated according to their location and thickness with respect to the neutral plane of the plate. For each sub-laminate, a set of nodes are generated according to the size of the delaminations, which are connected only with the elements for the respective sub-laminate. At the periphery of the each delamination, respective nodes

are merged with the nodes of sub-laminates, which are just below and above of the delamination.

3.4.3.1 Composite Plate with Magnetostrictive Sensor and Actuator

Numerical simulation is carried out by considering a laminated composite plate of total thickness 1.8mm as shown in Figure-3.11. Length and width of the beam is 500mm and 500mm respectively. The beam is made of 12 layers with thickness of each layer being 0.15 mm. Surface mounted magnetostrictive patches at the top and bottom layer are considered as actuator and sensor, respectively. Dimension of sensor and actuator are 100mm X 100mm and at the center of plate. Three center delaminations of size, 100mmX100mm, 200mmX200mm and 300mmX300mm are considered to study the effect of multiple delaminations in the response of structure. These delaminations are assumed just above the sensor, to block the direct stress waves from actuator to sensor. The FE modelling is done with the plate elements of 10 mm X 10 mm size. Solution is performed by Newmark time integration with 100 time steps.

Figure-3.12 shows the open circuit voltages for 50Hz actuation. Effect of coupling is less dominant than the effect of delamination, as the plate is severely damaged.

3.4.4 Finite Element Formulation of 2D Plane Strain Elements

In this subsection, as before, a 2-D plane strain Finite Element (FE) is deduced from the 3-D FE formulation. This element is then used to model different types of failures, namely the fiber breakages, internal cracks and matrix cracks. The main aim, as before, is to study the sensitivity of the response due to coupled and uncoupled model. Mechanical displacement fields can be written as

$$u(x,y,z,t) = u^0(x,z,t), \quad v(x,y,z,t) = 0, \quad w(x,y,z,t) = w^0(x,z,t), \tag{3.79}$$

where u, v, w are the components of mechanical displacement at location (x, y, z) in X, Y and Z direction respectively. u^0 and w^0 are the displacement components of the beam and depends on x, z and t. Magnetic fields in three coordinate directions are assumed as

$$H_x(x,y,z,t) = H^0_{xp}(x,z,t), \quad H_z(x,y,z,t) = H^0_{zp}(x,z,t), \quad H_y(x,y,z,t) = 0, \tag{3.80}$$

where, H^0_{xp} and H^0_{zp} are X and Z directional magnetic field of the magnetostrictive patch p respectively. The mechanical displacements and magnetic field component along the

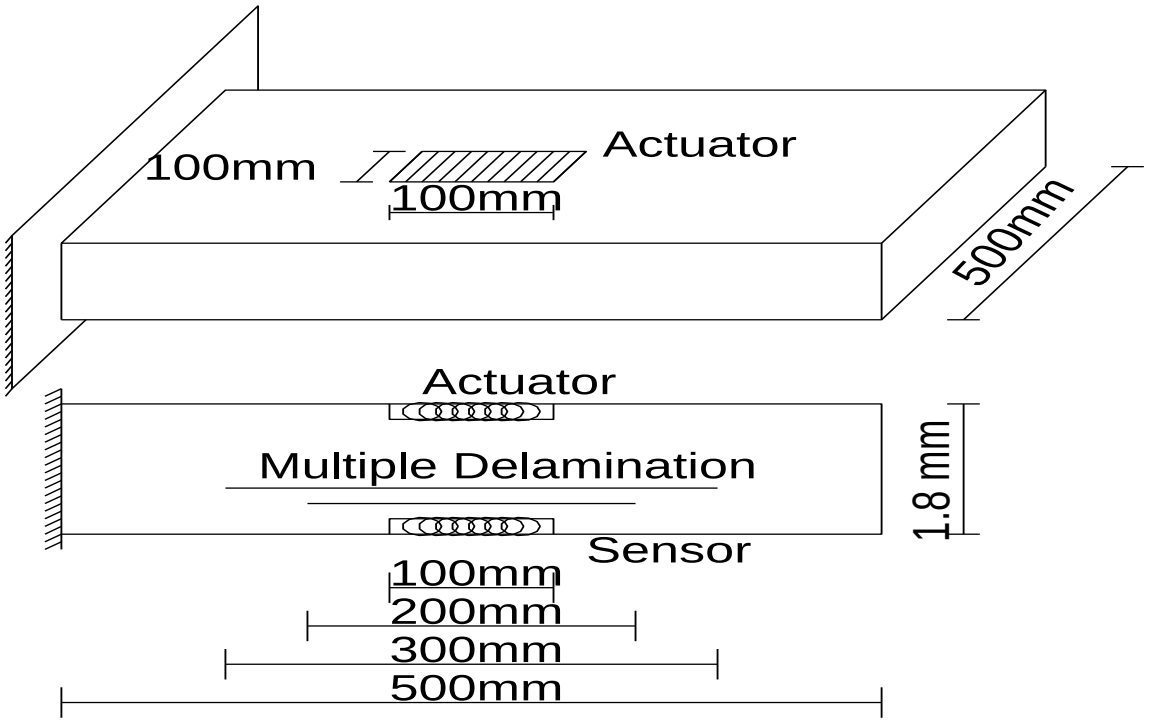

Figure 3.11: Multiple delaminated plate with magnetostrictive sensor and actuator

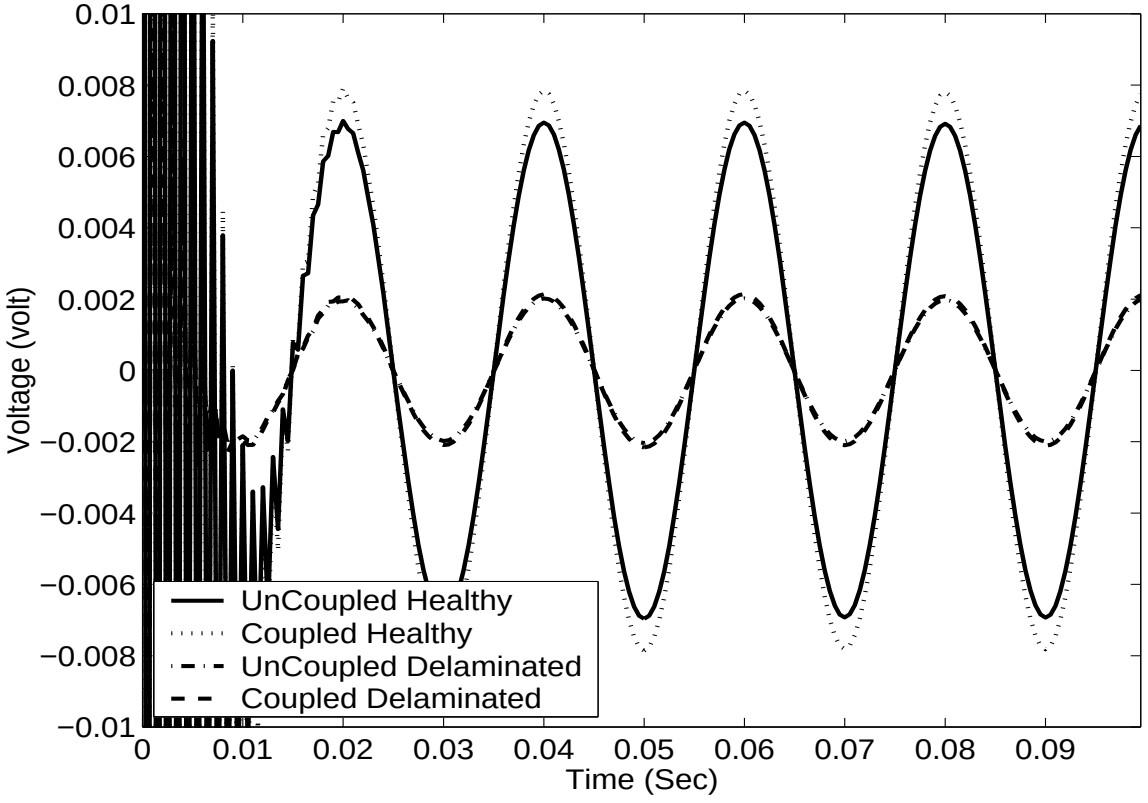

Figure 3.12: Sensor open circuit voltage for plate with multiple delaminations

width direction are assumed equal to zero. Stiffness and mass matrices for 2D plane strain element are derived using 4 noded bilinear shape functions with standard finite element formulation. Here each node of the element has four degrees of freedoms (two mechanical and two magnetic degrees of freedom).

3.4.4.1 Composite Beam with Different Types of Failure

Numerical simulation is carried out by considering a laminated cantilever composite beam of total thickness 20mm as shown in Figure-3.13. Length and width of the beam is 250mm and 50mm respectively. The beam is made of 4 layers ($[0/45/-45/90]$) with thickness of each layer being 5 mm. Surface mounted magnetostrictive patches at the top and bottom layer are considered as sensor and actuator, respectively. 50mm X 50mm X 5mm size sensor and actuator are placed near the support and 150mm apart from the support of the cantilever, respectively. Beam is modelled with 250 X 20 numbers of 4 noded plane strain elements with each size of 1 mm X1 mm. Thickness of the crack in FE modelling is assumed as 1 mm. Figure-3.13(a) shows the 5mm matrix cracking at 100 mm apart form the support. Matrix cracking in FE formulation is modelled by removing elements (5 numbers) from the location of the crack in the layer of 90^0 ply angle. Actuator is excited with 5kHz actuation. Figure-3.14 shows the open circuit voltages for this matrix cracking. Effect of matrix cracking is less sensitive than the error due to uncoupled material analysis. The stiffness loss at 90^0 layer is less compared to the 0^0 layer. Figure-3.13(b) shows the 5mm fiber breakage at 100mm apart form the support. Fiber breakage in FE formulation is modelled by removing elements (5 numbers) from the location of the crack in the layer of 0^0 ply angle. Figure-3.15 shows the open circuit voltages for this fiber breakage. Effect of fiber breakage is more sensitive than the error due to uncoupled material analysis. The stiffness loss at 0^0 layer is more compared to 90^0 layer in this case. Open circuit voltages are more for damaged structure than undamaged structure for both coupled and uncoupled formulation. Figure-3.13(c) shows the 10mm center crack at 100mm apart form the support. Center crack in FE formulation is modelled by removing elements (10 numbers) from the location of the crack. Figure-3.16 shows the open circuit voltages for this internal crack. In this case, the figure shows that the effect of damage and coupled formulation are comparable.

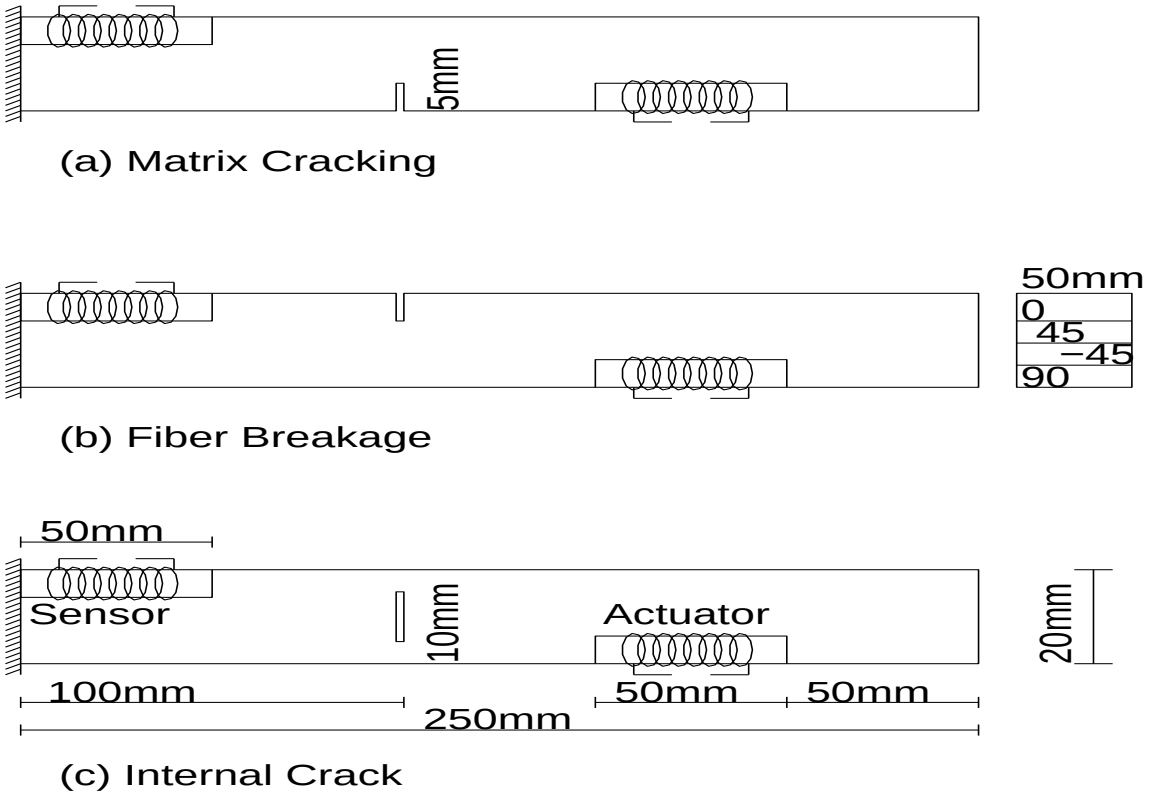

Figure 3.13: Laminated composite beam with sensor, actuator and crack

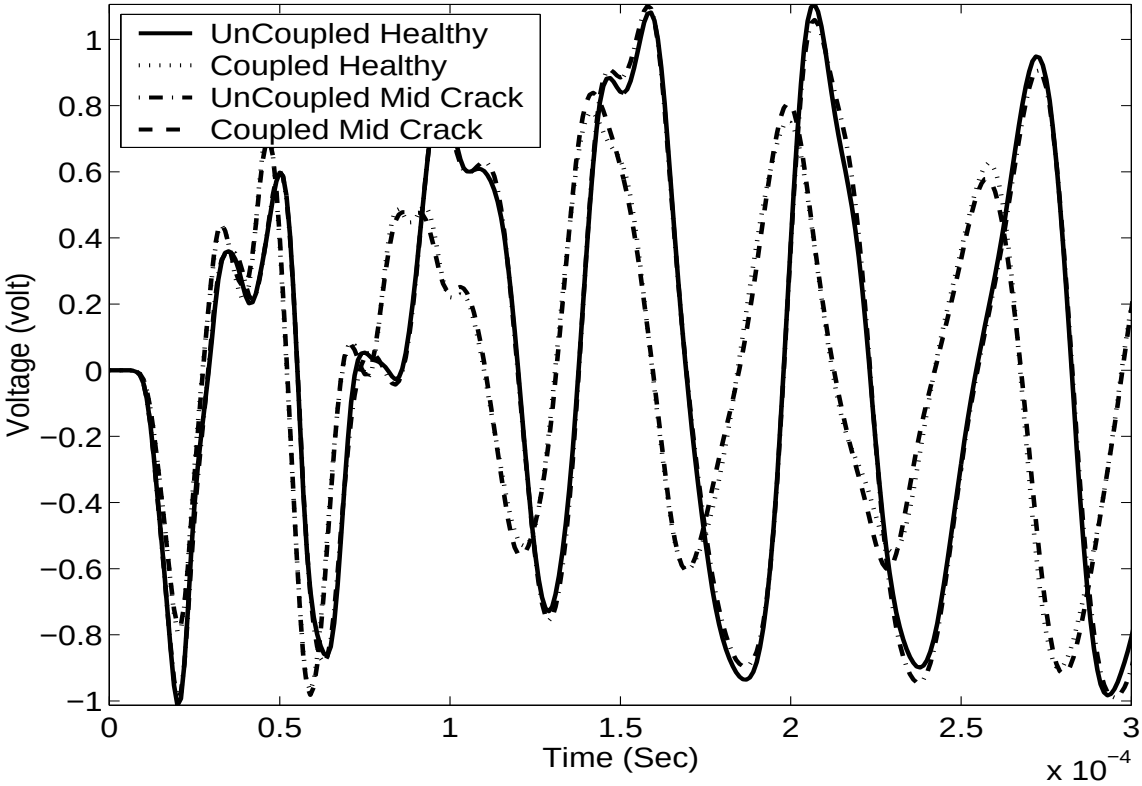

Figure 3.14: Sensor open circuit voltages for matrix crack in laminated composite beam

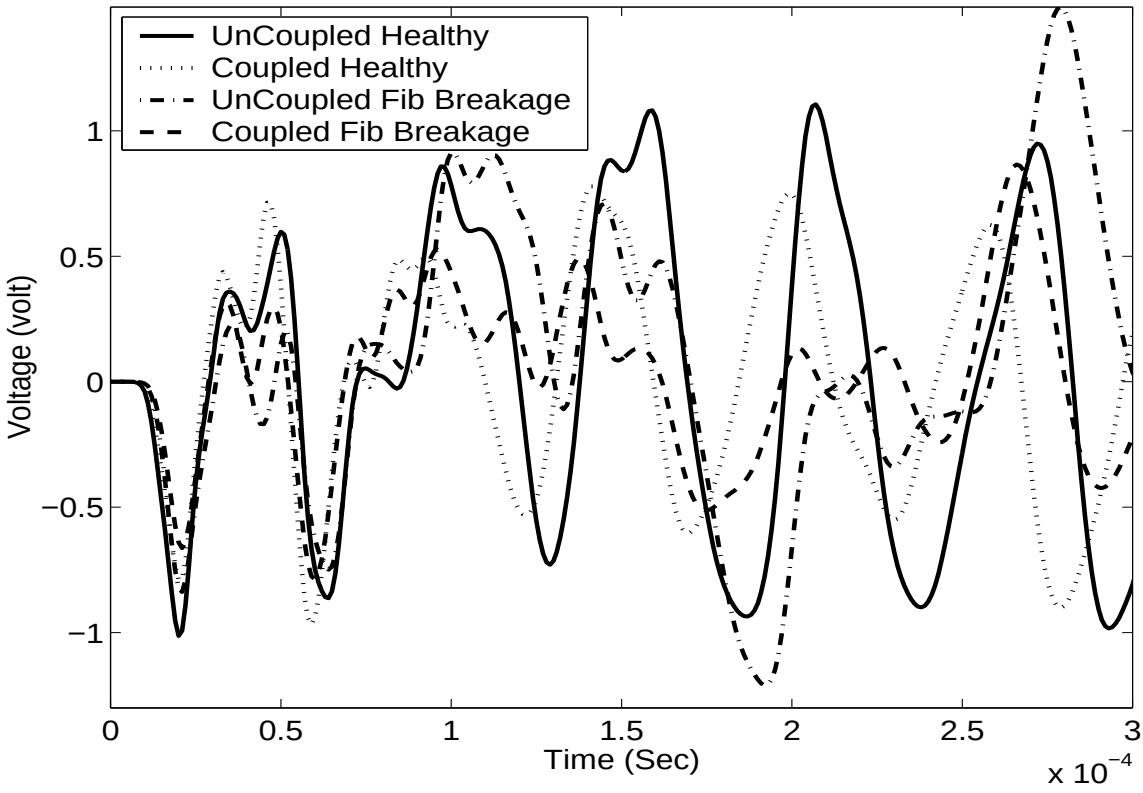

Figure 3.15: Sensor Open Circuit Voltages for Fiber Breakage

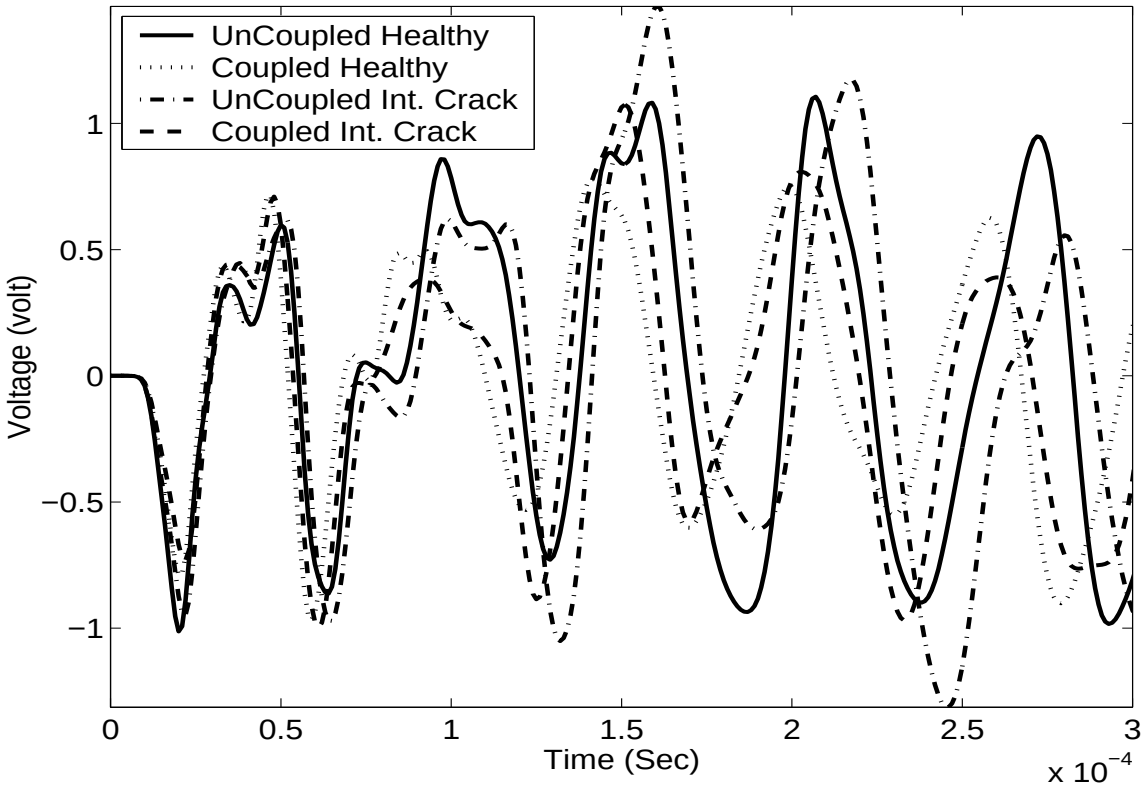

Figure 3.16: Sensor Open Circuit Voltages for Internal Crack

3.5 Summary

This study is mainly intended to bring out the importance of coupled model over uncoupled model in the analysis of smart composite structures with magnetostrictive patches and its effect on the structural health monitoring application. Coupled model is studied without assuming any direct relationship of magnetic field unlike uncoupled model. Here, elastic modulus, permeability and magneto-mechanical strain coefficient is considered as constant matrix. Actuation and sensing both has been done using actuation and sensing coil arrangement. Mechanical displacement and magnetic fields are considered as mechanical degrees of freedoms and smart degrees of freedoms respectively for finite element formulation. Thus both sensor and actuator coil properties can be incorporated with in the frame work of the finite element formulation. Numerical results have shown that coupling is quite significant for 90^0 ply angle and quite insignificant in a 0^0 laminate. Also, coupling is shown to be significant for low actuation frequency. It has been observed that the effect of coupling in static analysis is around 12% and is shown to increase with the thickness of the actuator. It is observed that for structural health monitoring application, coupled analysis is essential to get the true response of structure. However, when the damage is severe, simplified uncoupled analysis can still be used to get a preliminary solution.